# Northumbria Research Link

Citation: Shayanfar, Javad, Barros, Joaquim A.O. and Rezazadeh, Mohammadali (2023) Stress-strain model for FRP confined heat-damaged concrete columns. Fire Safety Journal, 136. p. 103748. ISSN 0379-7112

Published by: Elsevier

URL: https://doi.org/10.1016/j.firesaf.2023.103748 <https://doi.org/10.1016/j.firesaf.2023.103748 >

This version was downloaded from Northumbria Research Link: https://nrl.northumbria.ac.uk/id/eprint/51256/

Northumbria University has developed Northumbria Research Link (NRL) to enable users to access the University's research output. Copyright © and moral rights for items on NRL are retained by the individual author(s) and/or other copyright owners. Single copies of full items can be reproduced, displayed or performed, and given to third parties in any format or medium for personal research or study, educational, or not-for-profit purposes without prior permission or charge, provided the authors, title and full bibliographic details are given, as well as a hyperlink and/or URL to the original metadata page. The content must not be changed in any way. Full items must not be sold commercially in any format or medium without formal permission of the copyright holder. The full policy is available online: <a href="http://nrl.northumbria.ac.uk/policies.html">http://nrl.northumbria.ac.uk/policies.html</a>

This document may differ from the final, published version of the research and has been made available online in accordance with publisher policies. To read and/or cite from the published version of the research, please visit the publisher's website (a subscription may be required.)





# **1** Stress–strain Model for FRP Confined Heat-damaged Concrete Columns

2

Javad Shayanfar<sup>1</sup>, Joaquim A. O. Barros<sup>2</sup> and Mohammadali Rezazadeh<sup>3</sup>

<sup>1</sup> PhD Candidate, ISISE, Department of Civil Engineering, University of Minho, Azurém 4800-058 Guimarães, Portugal, <u>arch3d.ir@gmail.com</u> (corresponding author)

<sup>2</sup> Full Prof., ISISE, IBS, Department of Civil Engineering, University of Minho, Azurém 4800-058 Guimarães, Portugal, <u>barros@civil.uminho.pt</u>

<sup>3</sup> Lecturer, Civil Eng., Department of Mechanical and Construction Engineering, Northumbria University, Newcastle upon Tyne, NE1 8ST, United Kingdom, <u>mohammadali.rezazadeh@northumbria.ac.uk</u>

3

#### 4 Abstract:

5 This paper is dedicated to the development of a new analysis-oriented model to simulate the axial and 6 dilation behavior of FRP confined heat-damaged concrete columns under axial compressive loading. 7 The model's calibration has considered the experimental results from concrete circular/square cross-8 section specimens submitted to a certain level of heat-induced damage, which after attained the 9 environmental temperature, were fully confined with FRP jacket and tested. New equations were 10 developed to determine the mechanical characteristics of unconfined heat-damaged concrete by 11 performing regression analysis on a large database of experimental tests. Based on a parametric study 12 on dilation behavior of FRP confined heat-damaged columns, a new dilation model was developed to 13 predict concrete lateral strain at a given axial strain, dependent on the thermal damage level. By using 14 this dilation model, a new methodology was introduced for predicting the axial stress-strain response 15 of FRP confined heat-damaged columns in compliance with the active confinement approach. The 16 adequate predictive performance of the model is demonstrated by estimating experimental axial stress-17 strain results.

18 Keywords: FRP confined heat-damaged concrete; thermal damage; confinement model; dilation
19 behavior

20

#### 21 **1- Introduction**

During fire, concrete buildings generally demonstrate a better fire performance compared to 22 timber and steel buildings due to concrete non-combustibility and relatively low thermal 23 conductivity (Kodur [1], Bamonte and Lo Monte [2]). Nonetheless, depending on the fire 24 intensity imposed to the structural elements, material deteriorations occur during fire exposure, 25 resulting detrimental effects on the performance of concrete structures at their serviceability 26 and ultimate limit state conditions (Demir et al. [3]). Considering the pre-existing thermal-27 induced damage, a post-fire strengthening solution for restoring its structural performance can 28 be an environmental and economic sustainable solution over the demolishing and rebuilding 29 30 alternative. To reinstate sufficiently axial responses of heat-damaged concrete columns (HC), 31 externally bonded fiber-reinforced-polymer (FRP) composites have been demonstrated as a viable solution (Bisby et al. [4]). 32

33 Several experimental and analytical studies (i.e. Barros and Ferreira [5], Wang and Wu [6], Janwaen et al. [7], Shayanfar et al. [8]) were conducted to evaluate the capability of FRP 34 confining strategy in upgrading the axial and dilation behavior of FRP confined concrete 35 columns under axial compression at ambient conditions. For the case of FRP fully confined 36 concrete columns of circular cross section at ambient conditions (FFCC-A, as shown in Fig. 37 1a), Barros and Ferreira [5] experimentally evidenced that the confinement-induced 38 39 enhancements for normal-strength concrete is more pronounced than those registered in high-40 strength concrete. For the case of FRP fully confined concrete columns of square cross section at ambient conditions (FFSC-A, as shown in Fig. 1a), Wang and Wu [6] and Shan et al. [9] 41 conducted experimental studies to evaluate the influence of cross-section circularity in the 42 effectiveness of the confining strategy. It was evidenced that decreasing the corner radius (r)43 from r = b/2 (circular columns where b defines the length of the cross-section dimension) to r 44

45 = 0 (square columns with sharp edges) results in a significant reduction in terms of confinement
46 efficiency.

47 On the other hand, very limited experimental studies have been conducted for assessing the strengthening efficiency of FRP confining systems applied in the post-cooling regime of 48 49 concrete specimens subjected to a certain maximum exposure temperature according to the 50 heating scheme demonstrated in Fig. 1b. Bisby et al. [4] performed an experimental research 51 to assess the effectiveness of FRP fully confinement on circular concrete columns subjected to 52 different levels of maximum temperature (300, 500 and 700 °C) (FFCC-H, as shown in Fig. 53 1a). It was evidenced that FRP confinement could significantly increase the axial compressive strength and stiffness of unconfined heat-damaged specimens (Fig. 1c). The peak axial 54 compressive strength and the corresponding axial strain of FFCC-H specimens subjected to 55 severe thermal exposure (700 °C) were almost 90% and 145%, respectively, of those of FFCC 56 at ambient conditions. However, the secant axial stiffness of FFCC-H specimens (as the ratio 57 58 of axial stress to its corresponding axial strain) was reported to be considerably lower than that of FFCC, and this difference has increased with maximum exposure temperature  $(T_m)$ . Lenwari 59 et al. [10] experimentally evidenced that the axial stress versus axial strain response of FFCC-60 H is dependent on the used heating scheme, i.e.  $T_m$ , exposure duration and cooling regime (air 61 or water cooling methods), and on the axial compressive strength of AC, which was also 62 confirmed by Luo et al. [11]. Furthermore, it was shown that the level of axial strength 63 improvements, induced by FRP confining system, is higher in HC than in AC. Accordingly, 64 for HC with a high level of thermal damage, FRP effectiveness tends to be more significant. 65 66 Ouyang et al. [12] investigated experimentally the dilation behavior of heat-damaged circular concrete specimens confined by Basalt FRP (BFRP) jacket (FFCC-H) under axial compressive 67 loading. It was demonstrated that there is a noticeable difference between the transverse 68 expansibility of HC subjected to different level of the imposed  $T_m$ . Furthermore, the recorded 69

hoop strains at BFRP rupture were almost independent of the exposure temperature. Song *et al.* [13] experimentally evidenced the high potential of BFRP confining system for improving
the axial and dilation responses of HC with square cross-section (FFSC-H, as shown in Fig.
1a). The confinement-induced enhancements were more pronounced in HC exposed to high
temperatures and confined by thicker BFRP jackets.

75 For the prediction of the axial stress-strain response of FRP confined AC columns, several 76 analysis-oriented models, based on active confinement approach, have been recommended i.e. 77 Teng et al. [14], Lim and Ozbakkaloglu [15], and Shayanfar et al. [16 and 17]. Teng et al. [14] 78 proposed an analysis-oriented model for passively confined concrete, whose calibration was based on experimental observations in FRP fully confined concrete specimens of circular cross 79 section (FFCC). Based on theoretical principles and experimental evidences, Shayanfar et al. 80 [16] developed a generalized analysis-oriented model for passive confinement arrangements, 81 whose parameters were derived from the experimental results with FRP fully/partially confined 82 83 circular concrete specimens. Shayanfar et al. [17] extended Shayanfar et al. [16]'s model to make it applicable to the case of columns of square-cross section, by simulating the influence 84 of the non-circularity in terms of confinement-induced enhancements. Bisby *et al.* [4] proposed 85 86 a design-oriented model to determine the axial response of heat-damaged circular cross-section concrete columns confined by FRP (FFCC-H). In this model, the confinement-induced 87 improvements were expressed as a main function of maximum exposure temperature  $(T_m)$ 88 imposed to the column. Nevertheless, an analysis-oriented model to simulate the full-range of 89 dilation and axial responses of FRP fully confined HC columns with square cross-section is 90 91 still lacking.

92 This paper aims to introduce a new methodology to determine the axial stress-strain response
93 of FRP fully confined circular/square HC columns (the concrete specimens were submitted to

94 a certain  $T_m$ , and after having attained the environmental temperature, the fully confining FRP jacket was applied to the heat-damaged concrete). For the case of unconfined heat-damaged 95 concrete, through regression analysis performed on a large test database, new expressions are 96 97 developed to determine its mechanical characteristics in terms of axial compressive strength and its corresponding axial strain. By performing parametric studies with the available 98 experimental data, the significant influence of the pre-existing thermal-induced damage on the 99 100 establishment of the axial and dilation behavior of FRP fully confined heat-damaged concrete columns is demonstrated. By performing a parametric study to assess the influence of  $T_m$  on 101 102 the concrete transverse expansion, a new dilation model depending on the heat-damaged level is proposed, which has a unified character with the dilation model developed by Shayanfar et 103 104 al. [17] for concrete specimens at room temperature. By using the developed dilation model, a 105 new methodology is introduced, based on active confinement approach, for the simulation of 106 the axial stress-strain response of FRP fully confined circular/square HC columns at the different levels of  $T_m$ . The model's adequate predictive performance is demonstrated by 107 estimating experimental axial stress-strain responses. 108

109 2- Unconfined heat-damaged concrete columns (HC)

Kodur [1] evidenced that post-fire response of HC columns significantly depends on concrete 110 mechanical, thermal (including thermal conductivity, thermal diffusivity, specific heat, and 111 112 mass loss) and deformation (including concrete thermal expansion) properties, as well as on the spalling response. In general, concrete submitted to maximum exposure temperature  $(T_m)$ 113 up to 100 °C can be considered almost undamaged. Afterward, water loss (causing shrinkage) 114 and the expansion of aggregates induce internal stresses in the concrete, particularly for 115  $T_m \ge 300$  °C. Furthermore, thermal-induced chemical processes and thermo-mechanical 116 damages lead to a significant strength degradation for the concrete submitted to high levels of 117

exposure temperature [1]. A comprehensive review of concrete properties at elevated
temperatures can be found in Kodur and Sultan [18], Hertz [19], Raut and Kodur [20], Aslani
and Bastami [21].

In terms of mechanical properties, by submitting concrete to elevated temperature with a heating scheme including maximum exposure temperature  $(T_m)$ , the axial compressive stress of HC  $(f_c^T)$  and the modulus of elasticity  $(E_{cT})$  decrease depending upon its peak axial strength  $(f_{c0}^T)$ . However, axial strains corresponding to the peak  $(\varepsilon_{c0}^T)$  and ultimate stages  $(\varepsilon_{cu0}^T)$ increase, demonstrating a significant reduction on the axial stiffness (defined as  $f_c^T / \varepsilon_c$  where  $\varepsilon_c$  is the axial strain) of HC compared to AC (Hertz [19], Chang *et al.* [22], Al-Salloum *et al.* [23], Sharma *et al.* [24], Geng *et al.* [25], Xiao *et al.* [26], Xiang *et al.* [27]).

# 128 **2-1- Peak axial strength of HC** $(f_{c0}^T)$

Experimental studies evidenced that the heat-induced damages in HC columns lead to a reduction in terms of peak axial strength. Accordingly, by defining the axial strength ratio,  $\beta_{0T}$ , (the ratio of  $f_{c0}^{T}$  and  $f_{c0}$ ),  $f_{c0}^{T}$  can be expressed as:

$$f_{c0}^T = \beta_{0T} f_{c0} \tag{1}$$

132 The variation of  $\beta_{0T}^{Exp} = f_{c0}^{T}^{Exp} / f_{c0}^{Exp}$  with respect to  $T_m$  can be obtained from experimental 133 results of axial compression tests on HC columns. In the present study, a database of 292 HC 134 column specimens with a wide range of concrete properties and exposure temperature was 135 collected, as briefly presented in Table 1. The following criteria were adopted to 136 include/exclude experimental data: 1) ones obtained from circular/square/rectangular heat-137 damaged concrete specimens tested under concentric were included; 2) heat-damaged concrete 138 specimens subjected to a maximum exposure temperature more than 800 °C were excluded; 3)

Fig. 2a shows the variation of 
$$\beta_{0T}^{Exp}$$
 with respect to  $T_m$ , based on the results of the database,  
where a decrease of  $\beta_{0T}^{Exp}$  with the increase of  $T_m$ , from 1 to almost 0.2 corresponding to room  
conditions and 800 °C, respectively, is visible. Based on the best-fit relation obtained from  
regression analysis on the database information,  $\beta_{0T}$  versus  $T_m$  data can be obtained as  
 $\beta_{0T} = 1.087 - 0.00116T_m$ . By assuming *Error Index* as  $(1.087 - 0.00116T_m)/\beta_{0T}^{Exp}$ , Fig. 2b  
demonstrates that there is a slight variation in Error Index versus concrete strength relationship  
which is less than one up to almost  $f_{c0} = 110$  MPa, representing underestimation. However,  
beyond  $f_{c0} = 110$  MPa, the Error Index tend to be more than 1 resulting in overestimation of  
the experimental counterparts. Accordingly, based on regression analysis performed on the  
Error Index and concrete strength relationship,  $\beta_{0T}$  can be calculated by:

$$\beta_{0T} = \frac{1.087 - 0.00116T_m}{\gamma_f} \le 1 \tag{2}$$

153 in which

$$\gamma_f = 1 + (\gamma_0 - 1) \left( \frac{T_m - 25}{100} \right)$$
 for  $T_m \le 100 \text{ °C}$  (3a)

$$\gamma_f = \gamma_0 \qquad \qquad \text{for } T_m \ge 100 \text{ °C}$$
(3b)

$$\gamma_0 = 3415 \left(\frac{f_{c0}}{1000}\right)^3 - 721 \left(\frac{f_{c0}}{1000}\right)^2 + 44.5 \left(\frac{f_{c0}}{1000}\right) + 0.178 \tag{4}$$

where the developed expression is valid for  $T_m \leq 800$  °C based on the interval of the submitted maximum exposure temperatures ( $T_m = [25 \text{ °C}, 800 \text{ °C}]$ ) in the database used for the regression analysis.  $\gamma_0$  reflects the influence of  $f_{c0}$  (in MPa) in the determination of  $\beta_{0T}$ empirically.

In Fig. 2c, the results predicted by the proposed model are compared to those reported by the experiments (Table 2), with a mean = 0.964, a coefficient of variation (CoV) = 0.279, a mean absolute percentage error (MAPE) = 0.203, and an R-squared value ( $R^2$ ) = 0.876, revealing an acceptable predictive performance. Table 2 also shows that the proposed model provides a predictive performance better than of the existing models.

# 163 **2-2-** Axial strain at the peak stage of AC columns ( $\varepsilon_{c0}$ )

164 For the case of AC columns, the experimental and analytical studies conducted by [33-38] evidenced that  $\varepsilon_{c0}$  increases with the concrete compressive strength ( $f_{c0}$ ). Jansen and Shah 165 [34] experimentally demonstrated that the column aspect ratio ( $\lambda_L$  as the ratio of the column 166 height to its diameter) has also considerable influence on  $\mathcal{E}_{c0}$  due to the occurrence of strain-167 localization within a finite zone with a pronounced gradient of deformations due to the concrete 168 post-peak strain-softening behavior. In this study, in order to estimate  $\varepsilon_{c0}$ , a large database 169 (Table 3) was compiled from the experimental results available in the literature, resulting in 170 171 604 unconfined concrete specimens (AC) with a broad range of concrete properties and geometry configurations. Note that for the case of non-circular columns with a total cross-172 section area of  $A_g$ , based on Yang *et al.* [38] recommendations,  $\lambda_L$  can be determined as  $L/d_{eq}$ 173

where *L* is the columns' height and  $d_{eq}$  is the equivalent circular diameter ( $d_{eq} = \sqrt{4A_g/\pi}$ [38]).

Based on a preliminary sensitivity analysis, a low effect was achieved for the influence of the column size (i.e. the normalized  $d_{eq}/150$ , with  $d_{eq}$  in mm) to estimate  $\varepsilon_{c0}$  when compared to other influencing factors ( $f_{c0}$  and  $\lambda_L$ ). Accordingly, using regression analysis, the best-fit expression to predict  $\varepsilon_{c0}$  was derived as a function of  $f_{c0}$  and  $\lambda_L$  regardless of the column's cross-section dimension influence:

$$\mathcal{E}_{c0} = 0.0011 \left(\frac{f_{c0}}{\lambda_L}\right)^{0.25}$$
(5)

Table 4 evaluates the predictive performance of this relation with the results of the experimental tests, and also compares with that of existing models. Based on the assessment indicators (values of mean = 0.977, CoV = 0.184 and MAPE = 0.138), there is an acceptable agreement between model prediction and the experimental results. Furthermore, compared to the models recommended by Popovics [39], Karthik and Mander [40] and Lim and Ozbakkaloglu [41], it is the most accurate one, confirming its reliability.

# 187 **2-3-** Axial strain at the peak stage of HC columns ( $\varepsilon_{c0}^{T}$ )

The experiments with HC columns conducted by Chang *et al.* [22], Sharma *et al.* [24], Xiao *et al.* [26], Xiang *et al.* [27] evidenced that the axial strain  $(\varepsilon_{c0}^{T})$  corresponding to  $f_{c0}^{T}$  tends to increase significantly from  $\varepsilon_{c0}$  at ambient condition to  $\varepsilon_{c0}^{T} \gg \varepsilon_{c0}$  at elevated temperature, as shown in Fig. 3a.

The details of the experimental specimens in the assembled database, including 225 tested HCcolumns, is presented in Table 5.

194 The best-fit relation between  $\varepsilon_{c0}^{T Exp} / \varepsilon_{c0} - 1$  (representing the thermal damage-induced strain) 195 and  $T_m$  was obtained from regression analysis by considering the influence of  $f_{c0}$ , resulting:

$$\varepsilon_{c0}^{T} = \left(1 + 63f_{c0}^{-0.5} \left(\frac{T_{m}}{1000}\right)^{4.2}\right) \frac{\varepsilon_{c0}}{\alpha_{T}} \le 4.5 \frac{\varepsilon_{c0}}{\alpha_{T}}$$
(6)

in which

 $\alpha_T = 1 \qquad \qquad \text{for } T_m \le 100 \text{ }^{\circ}\text{C} \tag{7a}$ 

$$\alpha_T = 1.22 - 0.0025T_m + 3 \times 10^{-6} T_m^2 \qquad \text{for } T_m > 100 \text{ }^{\circ}\text{C} \tag{7b}$$

where the developed expression is valid for  $T_m \leq 800$  °C based on the interval of the submitted 197 maximum exposure temperatures  $(T_m = [25 \text{ °C}, 800 \text{ °C}])$  in the database used for the 198 regression analysis.  $\alpha_T$  is the calibration factor for the influence of  $T_m$  in the increase of axial 199 strain induced by thermal damage, obtained from the regression analysis. In Fig. 3b and Table 200 6, the predictive performance of this model is assessed based on 225 test specimen results. As 201 can be seen, Eq. (6) provides the most accurate model compared to the existing models in the 202 prediction of the experimental counterparts, even though conservative results were achieved 203 204 for some cases submitted to high level of exposure temperature.

## 205 3-Dilation behavior of FRP confined HC columns

## 206 **3-1-** Confinement pressure developed for ambient condition

For the case of FRP fully confined square AC columns (FFSC), based on the force equilibrium

at the cross-sectional level, confinement pressure  $(f_{l,f})$  generated by the FRP confining stress

209 ( $f_f$ ) can be expressed as (Shayanfar *et al.* [17]):

$$f_{l,f} = 2K_e \frac{n_f t_f}{D_{eq}} f_f \tag{8}$$

where  $n_f$  is the number of FRP layers; and  $t_f$  is the nominal thickness of one FRP layer. In Eq. (8),  $D_{eq}$  defines the diameter of the equivalent circular cross-section for columns of square cross section with *b* edge and *r* corner radius, which can be calculated as recommended by Shayanfar *et al.* [17]:

$$D_{eq} = \frac{1 - 0.215 R_b^2}{1 - 0.215 R_b} b \tag{a9}$$

214 where

$$R_b = 2r/b \tag{b9}$$

is the corner radius ratio. Note that by using  $D_{eq}$  in the determination of FRP confinement 215 pressure, FRP volumetric ratio in the equivalent circular cross-section would be identical to 216 that of original square cross-section column. In Eq. (8),  $K_{e}$  is the confinement efficiency factor. 217 Shayanfar et al. [17] modified the original concept of 'confinement efficiency factor' by 218 considering the impact of concrete expansion gradient in the establishment of confinement 219 220 pressure, besides the well-known phenomenon of arching action. By using this concept, the actual confinement pressure acting non-homogenously on the concrete is converted to an 221 222 equivalent confinement pressure with uniform distribution along transverse and longitudinal directions of the column. This factor includes two components, which can be determined as 223 suggested by Shayanfar et al. [17]: 224

$$K_e = K_H K_V \tag{10}$$

where  $K_{H}$  is the horizontal component, reflecting the influence of horizontal arching action on the distribution of confinement pressure within the cross-section of a non-circular columns (for circular columns,  $K_{H} = 1$ ), determined as:

$$K_H = R_b \ge 0.07 \tag{11}$$

In Eq. (10),  $K_v$  is the vertical component reflecting the influence of the gradient of concrete 228 lateral expansion along the column height, depending on the level of confinement stiffness (the 229 ratio of confinement pressure to concrete lateral strain). It was demonstrated by Shayanfar et 230 al. [16] that above a certain level of confinement stiffness, the confinement imposed to the 231 concrete is strong enough to strictly control the evolution of concrete expansion leading to an 232 almost null gradient along the vertical direction ( $K_v = 1$ ). However, for the cases with an 233 insufficient confinement stiffness, due to the lack of strong restriction in the curtailment of 234 concrete expansibility, the concrete column is expected to experience a highly non-235 homogenous distribution of concrete expansion and, consequently, the confinement pressure 236 in the axial loading direction is non-uniform. Shayanfar et al. [17] suggested a design-based 237 formulation to calculate  $K_V$  as follows: 238

$$K_V = \frac{1}{3} + \frac{2}{3}k_\varepsilon \tag{12}$$

239 in which

$$k_{\varepsilon} = 0.08 + 0.92 \left[ 2 \frac{I_f}{I_f^*} - \left(\frac{I_f}{I_f^*}\right)^2 \right] \le 1 \qquad \text{for } I_f \le I_f^*$$
(13a)

$$k_{\varepsilon} = 1$$
 for  $I_f > I_f^*$  (13b)

$$I_f^* = 0.06 + 0.0005 f_{c0} \tag{14}$$

$$I_{f} = 2K_{H} \frac{n_{f}t_{f}E_{f}\varepsilon_{c0}}{D_{eq}f_{c0}} \simeq K_{H} \frac{n_{f}t_{f}E_{f}}{550D_{eq}f_{c0}^{0.75}}$$
(15)

where  $k_{\varepsilon}$  represents the ratio of minimum and maximum concrete lateral expansion along the column height.  $I_f$  represents the confinement stiffness index regardless the influence of the gradient of concrete expansion along the column height. Finally,  $I_f^*$  is the confinement stiffness index above which  $K_V = 1$ , representing the homogenous concrete expansion along the column due to strong restrictions imposed to the concrete.

In this paper, for further simplification of the relative complexity of Eqs. (12-15) in the calculation of  $K_v$ , a simplified equation was developed based on a preliminary sensitivity analysis on the influencing factors in Eq. (12) as:

$$K_V = 2.2 \left( I_f \right)^{0.3} \le 1 \tag{16}$$

Accordingly, by using the design-based Eqs. (11, 15 and 16), the two components involved in  $K_e$  (Eq. (10)) can be calculated.

### 250 **3-2-** Confinement pressure developed for elevated condition

Based on the model developed for ambient conditions in the previous section, the confinement pressure  $(f_{l,f}^T)$  imposed by the FRP confining stress  $(f_f)$  to HC column can be expressed as:

$$f_{l,f}^{T} = 2K_{e}^{T} \frac{n_{f}t_{f}}{D_{eq}} f_{f}^{T}$$
(17)

253 in which

$$K_e^T = K_H K_V^T \tag{18}$$

where  $K_H$  can be determined by Eq. (11). Through the substitution of confinement stiffness index of FRP confined HC columns  $(I_f^T)$  with that of FRP confined AC ones  $(I_f)$  in Eq. (16),  $K_V^T$  can be expressed as:

$$K_V^T = 2.2 \left( I_f^T \right)^{0.3} = 2.2 \beta_{0T}^{-0.45} \left( I_f \right)^{0.3} \le 1$$
<sup>(19)</sup>

in which based on Eq. (15),

$$I_{f}^{T} = K_{H} \frac{n_{f} t_{f} E_{f}}{550 D_{eq} \left(f_{c0}^{T}\right)^{0.75}} = \beta_{0T}^{-0.75} I_{f}$$
(20)

where  $\beta_{0T}$  is the axial strength ratio calculated by Eq. (2), which is equal to 1 for concrete at ambient condition; Considering that  $f_f^T$  can be calculated as  $E_f \varepsilon_h^T = E_f \varepsilon_l^T$  (where  $\varepsilon_h^T$  and  $\varepsilon_l^T$ are the generated circumferential (hoop) and radial strains, respectively, and  $E_f$  is the FRP modulus elasticity), Eq. (17) is rearranged as:

$$f_{l,f}^{T} = 2K_{e}^{T} \frac{n_{f}t_{f}}{D_{eq}} E_{f} \varepsilon_{h}^{T}$$

$$\tag{21}$$

Based on Poisson's ratio effect ( $\varepsilon_h^T = \varepsilon_l^T = v_s^T \varepsilon_c$ , where  $v_s^T$  is the secant Poisson's ratio), Eq. (21) can be rearranged as:

$$f_{l,f}^{T} = 2K_e \frac{n_f t_f}{D_{eq}} E_f v_s^T \varepsilon_c$$
(22)

Accordingly, in order to calculate  $f_{l,f}^{T}$  imposed to the concrete at a certain level of  $\varepsilon_{c}$ , the corresponding  $v_{s}^{T}$  is required to be addressed, which will be presented in the following section.

266

#### 267 **3-3-Dilation mechanism at elevated conditions**

During axial compressive loading, after splitting cracks have occurred, by increasing the axial 268 strain, the development of concrete lateral expansion abruptly increases due to Poisson's ratio 269 effect. Experimental studies conducted by Barros and Ferreira [5], Mirmiran and Shahawy [46], 270 Lim and Ozbakkaloglu [47] and Zeng et al. [48] evidenced that the magnitude of concrete 271 272 dilatancy is strongly dependent on confinement stiffness imposed to the concrete. For the case of AC with a high level of confinement stiffness capable of limiting the evolution of concrete 273 expansion and splitting cracks, a remarkable enhancement in terms of axial strength and 274 deformability is obtained (Barros and Ferreira [5]). However, for the case of low confinement 275 stiffness, the confinement pressure imposed to the concrete is not able to overcome the concrete 276 tendency for abrupt expansion, leading to lower confinement-induced enhancements [49]. 277

For a preliminary assessment of the dilation response of FRP confined HC columns, the 278 experimental dilation results conducted by Ouyang et al. [12] are analyzed. All tests were 279 280 conducted with specimens of diameter and height of 150 mm and 300 mm, respectively. The 281 unconfined concrete compressive strength at the ambient condition was reported 45.1 MPa. Basalt FRP (BFRP) was used with the values of thickness, modulus of elasticity and rupture 282 strain of 0.121 mm, 108.3 GPa and 2.18%, respectively. The HC columns were subjected 283 initially to various levels of maximum temperature (200 °C, 400 °C, 600 °C and 800 °C). Then, 284 they were fully confined with two and four layers of BFRP. Fig. 4 demonstrates the 285 experimental dilation responses of BFRP confined HC specimens reported by Ouyang et al. 286 [12]. Here,  $\varepsilon_v$  is the volumetric strain determined as  $\varepsilon_v = \varepsilon_c - 2\varepsilon_l = (1 - 2v_s)\varepsilon_c$  in which  $v_s$  is 287 the secant Poisson's ratio as  $v_s = \varepsilon_l / \varepsilon_c$ . Moreover, the negative and positive values of  $\varepsilon_v$ 288 represent volumetric expansion and contraction, respectively. To better demonstrate the 289 contribution of thermal-induced damage level in terms of dilation behavior, the model 290

developed by Shayanfar *et al.* [8 and 17] was followed to determine the dilation results associated with FRP confined AC specimens (*T25-L2* and *T25-L4* with red solid lines). Note that Ti-Lj refers to the concrete column heated up to the i-th maximum exposure temperature (Ti) and then, confined by j layers of BFRP.

As can be seen in Fig. 4, for all cases, regardless the level of thermal-induced damage, initial 295 296 behavior up to transition zone is virtually the same. However, beyond the transition zone, there is a noticeable difference between the transverse expansibility of HC and AC specimens. Fig. 297 298 4a reveals that at a certain axial strain ( $\varepsilon_c$ ), lateral strain ( $\varepsilon_l$ ) for the cases of T200-L2 and T400-L2 was obtained significantly higher than that of T25-L2, demonstrating the effect of 299 thermal damage on increase of  $\varepsilon_i$ . Likewise, from Fig. 4b, T200-L2 and T400-L2 have 300 experienced a large incremental volumetric expansion. However, in the T25-L2, beyond 301  $\varepsilon_c = 0.008$ , a considerable decrease in the magnitude of the increase in volumetric strain ( $\varepsilon_v$ ) 302 with respect to  $\varepsilon_c$ , followed by a reverse in volumetric evolution around  $\varepsilon_c$  =0.02, reveals the 303 capability of the confinement system imposed to AC column (T25-L2) in limiting the 304 transverse expansibility of AC columns. Likewise, as demonstrated in Fig. 4c, for T25-L2, due 305 to the adequate activated confinement imposed to AC column to overcome its tendency for 306 lateral expansibility, beyond the peak stage,  $v_s$  trend followed a decreasing branch. Even 307 308 though, heat-induced expansion for HC columns leads to an earlier activation in passive confining system of T200-L2 and T400-L2, the applied confinement was not adequate to 309 strongly constrain the concrete expansion evolution, based on its abrupt increase in  $v_s$  after 310 transition zone. On the other hand, for the cases subjected to high level of temperature (T600-311 L2 and T800-L2), as shown in Fig. 4a, at a certain level of  $\varepsilon_1$ , T600-L2 and T800-L2 312 experienced a larger axial deformation depending on thermal damage level, compared to T25-313 L2, T200-L2 and T400-L2. Likewise, Fig. 4b reveals that up to a certain level of axial strain, 314

315 the changes in volumetric evolution for T600-L2 and T800-L2 were almost marginal, while they underwent large axial deformations. Nonetheless, above this axial strain level, as a 316 consequence of the degeneration of micro- into meso- and macro-cracks along with heat-317 induced damage in the concrete, the volumetric change evolution was suddenly reversed 318 triggering an abrupt increase in volumetric expansion. Fig. 4c also shows that for T600-L2 and 319 T800-L2, compared to the other cases, larger axial strains were obtained for a certain Poisson's 320 ratio. Furthermore, a closer evaluation of the data demonstrates that the maximum secant 321 Poisson's ratio decreases significantly with increasing thermal damage, which can be attributed 322 323 to the substantial contribution of the heat-induced damage level in the establishment of dilation behavior of HC. Accordingly, by applying a certain level of axial loading, the heat-induced 324 damage leads to an additional axial strain in HC columns, and alters their transverse 325 326 expansibility, dependent strongly on thermal damage level. The comparison of dilation responses shown in Fig. 4a and Fig. 4d confirms a significant reduction in terms of lateral strain 327 by increasing FRP thickness (confinement stiffness), predominantly beyond the transition 328 zone. Fig. 4e reveals that an increase in confinement stiffness leads to shorter volumetric 329 expansion due to the stronger restrictions imposed to the concrete expansibility. The relations 330 of  $v_s$  and  $\varepsilon_c$  shown in Fig. 4f also confirms this behavior, where the specimens with more FRP 331 332 thickness experienced a lower value of  $v_s$  than those with less thickness (Fig. 4c).

333	In this study, it is aimed to extend the dilation model of Shayanfar et al. [8,17] originally
334	suggested for FRP confined AC specimens to the case of FRP confined HC column through
335	formulating the relation between $v_s^T$ and $\varepsilon_c$ at different levels of heat-induced damage $(T_m)$
336	based on regression analysis. For this purpose, a dataset of the dilation responses obtained from
337	existing experimental data was collected as presented by Table 7. It should be noted that the
338	following criteria were adopted to include/exclude experimental data: 1) ones obtained from

concentric loading tests were included; 2) Specimens with a full confinement of unidirectional  
fibers installed transversely to the axial compression direction were included; 3) Specimens  
with helical wrapping configuration or hybrid confinement arrangements were excluded; 4)  
specimens of rectangular cross-section with transverse and longitudinal steel reinforcements  
were excluded; 5) ones registered experimentally with incomplete documented information,  
i.e. maximum exposure temperature, geometry details and material properties, were excluded;  
6) ones obtained from test specimens with a premature failure mode caused by FRP debonding  
were excluded. In this table, 
$$v_{s,max}^{T}$$
 represents the peak Poisson's ratio of HC columns confined  
by FRP.  $\eta_T$  defines the ratio of  $v_{s,max}^{T}$  to  $v_{s,max}^{A}$  (where  $v_{s,max}^{A}$  is the peak Poisson's ratio of FRP  
study, the confinement stiffness-based model developed by Shayanfar *et al.* [17] was followed,  
which is determined as a main function of the confinement stiffness ( $\rho_{K,f}$ ), namely:

$$v_{s,\max}^{A} = \frac{0.25}{\left(1 + L_{d0}/D_{eq}\right)\sqrt{\rho_{K,f}}}$$
(23)

351 in which (by considering Eqs. (10), (15) and (16))

$$\rho_{K,f} = K_V I_f = K_e \frac{n_f t_f E_f}{550 D_{eq} f_{c0}^{0.75}}$$
(24)

$$0.57 \le \frac{L_{d0}}{\sqrt{A_g}\psi_f} = 1.71 - 3.53 \times 10^{-5} A_g \le 1.36$$
<sup>(25)</sup>

$$\psi_f = \frac{6.3}{\sqrt{f_{c0}}} \le 1$$
(26)

- where  $L_{d0}$  is the compression damage zone length of unconfined concrete columns which was determined as recommended by Lertsrisakulrat *et al.* [50];  $A_g$  is the total area of the column's cross section.
- For the determination of  $v_{s,\max}^T$ , it can be considered a function of  $v_{s,\max}^A$  by

$$v_{s,\max}^{T} = \frac{v_{s,\max}^{T}}{v_{s,\max}^{A}} v_{s,\max}^{A} = \eta_{T} v_{s,\max}^{A}$$
(27)

Therefore, by calculating 
$$v_{s,\text{max}}^{A}$$
 using Eq. (23) for the specimens assembled in the database,  
their corresponding values of  $\eta_{T}$  can be obtained as  $\eta_{T}^{Exp} = v_{s,\text{max}}^{T} / v_{s,\text{max}}^{A}$  (Table 7). Fig. 5a  
shows the variation of  $\eta_{T}^{Exp}$  with respect to  $T_{m}$ . As can be seen, by increasing  $T_{m}$  in the interval  
25–400 °C,  $\eta_{T}^{Exp}$  significantly increases up to the peak, while for  $T_{m} > 400$  °C, a noticeable  
reduction of  $\eta_{T}^{Exp}$  with the increase of  $T_{m}$  is observed. Based on the best-fit relation obtained  
from regression analysis performed on 78 experimental data, the following equation was  
derived for determining  $\eta_{T}$  from  $T_{m}$  and  $R_{b}$  (Fig. 5a):

$$\eta_{T} = \frac{33.2 \left(\frac{T_{m}}{1000}\right)^{3} - 51 \left(\frac{T_{m}}{1000}\right)^{2} + 21.2 \left(\frac{T_{m}}{1000}\right) - 0.49}{1.65 - 0.65R_{b}} \ge 1 \qquad \text{for } T_{m} \le 100 \text{ }^{\circ}\text{C}$$
(28a)

$$\eta_T = \frac{33.2 \left(\frac{T_m}{1000}\right)^3 - 51 \left(\frac{T_m}{1000}\right)^2 + 21.2 \left(\frac{T_m}{1000}\right) - 0.49}{1.65 - 0.65R_b} \le 2 \qquad \text{for } 100 \text{ }^\circ\text{C} < T_m \le 800 \text{ }^\circ\text{C}$$
(28b)

where the developed expression is valid for 
$$T_m \le 800$$
 °C based on the interval of the submitted  
maximum exposure temperatures ( $T_m = [25 \text{ °C}, 800 \text{ °C}]$ ) in the database used for the  
regression analysis. Therefore, by addressing  $v_{s,\max}^A$  and  $\eta_T$  in Eq. (27) through Eqs. (23, 28),

the peak Poisson's ratio of FRP confined HC columns 
$$(v_{s,\text{max}}^T)$$
 can be calculated. Fig. 5b  
evaluates the performance of Eq. (27). Based on the obtained assessment indicators, the  
established expression revealed a good predictive performance.

- For the determination of Poisson's ratio of HC columns confined by FRP  $(v_s^T)$  during axial
- 370 loading,  $v_s^T$  is considered as a function of  $v_{s,\max}^T$ , resulting in

$$v_s^T = \frac{v_s^T}{v_{s,\max}^T} v_{s,\max}^T = \eta_\varepsilon v_{s,\max}^T$$
(29)

371 where  $\eta_{\varepsilon}$  represents the ratio of  $v_s^T$  and  $v_{s,\max}^T$  at a given axial strain ( $\varepsilon_c$ ). Introducing Eq. (27)

# 372 into Eq. (29), $v_s^T$ is suggested by

$$v_s^T = \eta_\varepsilon \eta_T v_{s,\max}^A \tag{30}$$

- To calculate  $v_s^T$  by Eq. (30),  $\eta_{\varepsilon}$  needs to be addressed as an input parameter. For the
- determination of  $\eta_{\varepsilon}$  at a given level of  $\varepsilon_{c}$  for FRP confined AC columns (at ambient

- Fig. 6a. in this figure,  $c_0 c_1, c_2, c_3, c_4$  and  $c_5$  are the calibration factors reflecting the influence
- 377 of confinement stiffness on  $\eta_{\varepsilon}$  versus  $\varepsilon_{c}$  relation;  $\varepsilon_{c,m}$  represents the axial strain

378 corresponding to 
$$v_{s,max}^A$$
;  $v_{s,0}$  is the initial Poisson's coefficient of unconfined AC columns,

which was determined by (Candappa *et al.* [51]):

$$v_{s,0} = 8 \times 10^{-6} f_{c0}^{2} + 2 \times 10^{-4} f_{c0} + 0.138$$
(31)

As can be seen in Fig. 6a, the pre- and post-peak phases are dependent of  $\rho_{K,f}$ . The pre-peak

381 relation demonstrates that concrete initially behaves similar to unconfined AC column with

initial Poisson's coefficient as 
$$v_{s,0}$$
. Afterward ( $\varepsilon_c > \varepsilon_{c0}$ ),  $\eta_{\varepsilon}$  increases up to the peak stage (  
 $\eta_{\varepsilon} = 1$ ) at  $\varepsilon_{c,m}$ . The post-peak relation shows that  $\eta_{\varepsilon}$  decreases with the increase of  $\varepsilon_c$ , whose  
reduction magnitude is dependent on  $\rho_{K,f}$ . In the present study, the relation developed by  
Shayanfar *et al.* [8] was extended for the case of FRP confined HC columns. For this purpose,  
as presented in Fig. 6b, a new relation of  $\eta_{\varepsilon}$  versus  $\varepsilon_c$  was developed where the influence of  
thermal damage was reflected by the parameter  $\beta_{\varepsilon}$ .

$$\beta_{\varepsilon} = \beta_{\rho} \left( \varepsilon_{c0}^{T} - \varepsilon_{c0} \right) \tag{32}$$

388 in which

$$0.4 \le \beta_{\rho} = 11 \rho_{K,f}^{0.75} \le 1.4 \tag{33}$$

Accordingly, by calculating  $\beta_{\varepsilon}$  through Eq. (32),  $\eta_{\varepsilon}$  at a given  $\varepsilon_{c}$  can be obtained from the

data presented in Fig 6b. Then, the corresponding  $v_s^T$  can be calculated by Eq. (30). To evaluate

the reliability of the proposed relation, the results obtained from the experiments conducted by

Ouyang *et al.* [12] and those determined by Eq. (30) are compared Fig. 7. As can be seen, the

393 model has a good agreement with the experimental counterparts.

- 394 To obtain  $\varepsilon_l^T$  versus  $\varepsilon_c$  response of FFCC-H/FFSC-H based on the developed dilation model,
- 395 the calculation procedure is summarized as:
- **1.** Determine  $K_e$  using Eqs. (10), (11) and (16)
- 397 **2.** Determine  $\rho_{K,f}$  using Eq. (24)
- **398 3.** Determine  $v_{s,\max}^A$  using Eqs. (23)
- 399 **4.** Determine  $\eta_T$  using Eq. (28)

- 400 5. Assume a value for axial strain ( $\varepsilon_c$ )
- 401 **6.** Determine  $\beta_{\varepsilon}$  using Eqs. (32), (5) to (7)
- 402 7. Determine  $\eta_{\varepsilon}$  using the developed multilinear model in Fig. 6b
- 403 **8.** Determine  $v_s^T$  using Eq. (29)
- 404 **9.** Determine  $\varepsilon_l^T$  as  $\varepsilon_l^T = v_s^T \varepsilon_c$
- **10.** Continue the steps 5 to 9 up to the aim maximum value of  $\varepsilon_c$ , resulting a  $\varepsilon_l^T$  versus  $\varepsilon_c$ relation.

For the assessment of the model capability in the prediction of dilation response, Fig. 8 compares  $\varepsilon_l^T$  versus  $\varepsilon_c$  relations extracted from the experimental tests conducted by Ouyang *et al.* [12] and those simulated by the proposed model. As shown, the experimental results were simulated suitably by the model confirming its reliable predictive performance.

#### 411 4- Axial Compressive Stress-strain Relation

Fig. 9 demonstrates the remarkable influence of the exposure temperature on the axial response 412 of HC columns fully confined by FRP, tested by Bisby et al. [4] and Ouyang et al. [12]. As can 413 414 be seen in Fig. 9a for the case of the results reported by Bisby et al. [4], compared to T25-L1 (control experimental specimen), even though T300-L1 experienced a slight heat-induced 415 reduction in terms of initial axial stiffness, it showed higher axial strength and deformability. 416 417 For T500-L1, heat- induced damage did not lead to a significant difference in the axial stress versus axial strain relationship. However, for the case of severely heat-damaged specimens 418 (T686-L1), there is a noticeable reduction in its axial stiffness, compared to T25-L1. Moreover, 419 the axial stress versus axial strain relationship of T686-L1 was almost linear, compared to 420 almost bi-linear curves of specimens with the exposure temperatures lower than or equal to 500 421 °C. From the secant axial stiffness versus axial strain curves in Fig. 9b, T25-L1, T300-L1 and 422

423 T500-L1 presented a reduction of the axial stiffness during the axial compressive loading. However, in T686-L1, after an initial relatively small reduction of the stiffness, it was preserved 424 almost constant during the loading process, a consequence of the confinement effect provided 425 426 by the FRP. The assessment of the exposure temperature effects on the test specimens conducted by Ouyang et al. [12] revealed that the axial strength and stiffness of specimens 427 subjected up to 400 °C were higher than of T25-L2. It can be attributed to earlier activation of 428 confining system in the cases of HC than AC due to the increase of concrete expansibility 429 430 caused by the heat-induced damage. However, by increasing the temperature above that limit of 400 °C, thermal-induced damage increases significantly the axial deformation of the 431 concrete specimen, converting a bi-linear stress-strain response into a linear one (Fig. 9c), and 432 consequently an almost constant axial stiffness during axial loading process (Fig. 9d). 433 Accordingly, the experimental results presented in Fig. 9 evidence the imperious impact of 434 exposure maximum temperatures on the axial stress-strain response of FRP confined HC 435 columns. 436

In order to calculate the axial stress versus axial strain relationship ( $f_c^A$  vs  $\varepsilon_c$  curve) of FRP 437 passively confined AC columns (passively-confined-concrete), Active Confinement Approach 438 (i.e. [14-17, 52-54] can be followed. In this approach, the axial response of concrete with 439 440 passive confinement is derived based on that of actively-confined-concrete subjected to a constant confinement pressure during the entire axial loading history. Accordingly,  $f_c^A$ 441 corresponding to  $\varepsilon_c$  at a certain level of FRP confinement pressure  $(f_{l,f}^{A})$  can be calculated 442 by adopting an axial stress-strain base relation model  $(f_c^A = g_1(f_{cc}^A, \varepsilon_c))$  coupled with an axial 443 strength model, also known as failure surface function,  $(f_{cc}^{A} = g_2(f_{l,f}^{A}))$  developed for 444 actively-confined-concrete. Here,  $f_{cc}^{A}$  is the peak axial strength of axial stress-strain base 445

relation model (defined from function  $g_1$ ). However, since actively-confined-concrete case is 446 under a constant  $f_{l,f}^{A}$  during the entire axial loading history, contrary to passively-confined-447 concrete, the studies [15-17] evidenced that the original Active Confinement Approach 448 449 overestimates the FRP-induced enhancement of passively-confined-concrete, which is generally recognized as *Confinement Path Effect*. To consider this effect, by adopting functions 450  $g_1$  and  $g_2$  from those exclusively developed for actively-confined-concrete, Lim and 451 452 Ozbakkaloglu [15] recommended a reduction factor in the confinement-induced enhancements obtained for actively-confined-concrete, by decreasing the level of the confinement pressure 453  $f_{l,f}^{A}$  in the function g<sub>2</sub>. Shayanfar *et al.* [16 and 17] proposed a new axial strength framework 454 model (function  $g_2$ ) exclusively suggested for passively-confined-concrete to predict 455 456 enhancements offered by a passive confining system.

In the present paper, for the calculation of  $f_c^A$  and  $\varepsilon_c$  relation of FRP confined AC columns taking into account *confinement path effect*, the model developed by Shayanfar *et al.* [17] presenting a unified character for both full and partial confinement configurations and both circular and square cross-sections, is followed. In this model, the axial stress-strain base framework ( $f_c^A$  versus  $\varepsilon_c$  relation using function  $g_l$ ) is given by:

$$f_{c}^{A} = f_{cc}^{A} \frac{\left(\varepsilon_{c}/\varepsilon_{cc}^{A}\right)n_{A}}{n_{A} - 1 + \left(\varepsilon_{c}/\varepsilon_{cc}^{A}\right)^{n_{A}}}$$
(34)

462 in which

$$\frac{f_{cc}^{A}}{f_{c0}} = 1 + \frac{R_{1}}{R_{2}} \left(\frac{f_{l,f}^{A}}{f_{c0}}\right)^{R_{2}}$$
(35)

$$\frac{\varepsilon_{cc}}{\varepsilon_{c0}}^{A} = 1 + 5 \left( \frac{f_{cc}}{f_{c0}}^{A} - 1 \right)$$
(36)

$$n_{A} = \frac{E_{c}}{E_{c} - \frac{f_{cc}}{\varepsilon_{cc}^{A}}} \approx \frac{1}{1 - 2.1 \times 10^{-4} \psi_{A}} \ge 1.1$$
(37)

$$\Psi_A = \frac{f_{cc}^{\ A}}{\varepsilon_{cc}^{\ A} \sqrt{f_{c0}}}$$
(38)

where  $f_{cc}^{A}$  and  $\varepsilon_{cc}^{A}$  are the peak axial strength and its corresponding axial strain, calibrated based on experimental AC specimens with passively confining system;  $R_1$  and  $R_2$  are the calibration factors in the determination of  $f_{cc}^{A}$ ;  $n_A$  is the concrete brittleness at the ambient condition depending on  $\psi_A$ , as recommended by Carreira and Chu [55]. Accordingly, at a certain level of  $\varepsilon_c$ ,  $f_{cc}^{A}$  can be determined as a function of  $f_{l,f}^{A}$  based on Eq. (35), and  $\varepsilon_{cc}^{A}$ can be, subsequently, calculated by Eq. (36), as input parameters for the determination of  $f_{c}^{A}$ by Eq. (34).

In this study, the model developed by Shayanfar *et al.* [17] was extended to be applicable for the establishment of axial response of the concrete being subjected to a certain exposure temperature. Accordingly, by substituting the mechanical characteristics of HC column with those of AC column, at a certain level of  $\varepsilon_c$  leading to FRP confinement pressure  $(f_{l,f}^T)$ , axial stress-strain base relation model  $(f_c^T$  versus  $\varepsilon_c$  curve using function  $g_l$ ) can be expressed as:

$$f_c^T = f_{cc}^T \frac{\left(\varepsilon_c / \varepsilon_{cc}^T\right) n_T}{n_T - 1 + \left(\varepsilon_c / \varepsilon_{cc}^T\right)^{n_T}}$$
(39)

475 in which

$$n_T = \frac{1}{1 - 2.1 \times 10^{-4} \psi_T} \ge 1.1 \qquad \text{for } T_m \le 400 \text{ }^{\circ}\text{C}$$
(40a)

$$n_T = 2 - \frac{1 - 4.2 \times 10^{-4} \psi_T}{1 - 2.1 \times 10^{-4} \psi_T} \left( 2 - \frac{T_m}{400} \right) \ge 1.1 \qquad \text{for } 400 \ ^\circ\text{C} \le T_m \le 800 \ ^\circ\text{C}$$
(40b)

$$\Psi_T = \frac{f_{cc}^T}{\varepsilon_{cc}^T \sqrt{f_{c0}^T}} \tag{41}$$

where  $f_{cc}^{T}$  and  $\varepsilon_{cc}^{T}$  are the peak axial strength and its corresponding axial strain at a certain 476 level of  $\varepsilon_c$  as input parameters for the axial stress-strain base relation model.  $n_T$  is the concrete 477 brittleness that considers the influence of the maximum exposure temperature on  $f_{cc}^{T}$ ,  $\varepsilon_{cc}^{T}$  and 478  $f_{c0}^{T}$  through the parameter  $\psi_{T}$ . Note that the axial stiffness of FRP confined HC columns with 479 severe thermal-induced damages ( $T_m \simeq 600-800$  °C) seems to be almost constant with a linear 480 axial behavior during axial loading as demonstrated in Fig. 9. Accordingly, in the present study, 481  $n_T$  corresponding to  $T_m = 800$  °C was assumed equal to a constant value of  $n_T = 2$  during the 482 entire loading history, adjusted based on the best-fit relation of the proposed model with the 483 484 experimental axial stress-strain responses reported by Bisby et al. [4], Lenwari et al. [10], Ouyang et al. [12] and Song et al. [13]. Consequently, in Eq. (40b) (400 °C  $\leq T_m \leq 800$  °C), 485  $n_T$  was considered on the interval of the  $n_T$  obtained from Eq. (40a) for  $T_m = 400$  °C and 486  $n_T = 2$  corresponding to  $T_m = 800$  °C, with a linear relationship with  $T_m$ . 487

For the establishment of  $\varepsilon_{cc}^{T}$  at high temperatures, the preliminary comparative assessment of the proposed model with  $\varepsilon_{cc}^{T}$  obtained based on Eq. (36) demonstrated a very significant underestimation in its model predictive performance, particularly for the cases with severe thermal-induced damages. On the other hand, based on experimental studies it was evidenced that the axial behavior of FRP confined HC columns tends to be similar to actively-confined493 concrete due to more expansive behavior of HC than AC (Fig. 4). Therefore, the  $\varepsilon_{cc}^{T}$  of HC 494 columns with high exposure temperature is calculated according to the approach proposed by 495 Lim and Ozbakkaloglu [41], exclusively developed for the case of actively-confined-concrete:

$$\varepsilon_{cc}^{T} = \varepsilon_{c0}^{T} \left[ 1 + 5 \left( \frac{f_{l,f}^{T}}{f_{c0}^{T}} - 1 \right) \right] \qquad \text{for } T_{m} \ge 100 \text{ }^{\circ}\text{C}$$

$$(42a)$$

$$\varepsilon_{cc}^{T} = \varepsilon_{c0}^{T} + 0.045 \left(\frac{f_{l,f}^{T}}{f_{c0}^{T}}\right)^{1.15} + \lambda_{\varepsilon} \qquad \text{for } 100 \ ^{\circ}\text{C} \le T_{m} \le 200 \ ^{\circ}\text{C} \qquad (42b)$$

$$\varepsilon_{cc}^{T} = \varepsilon_{c0}^{T} + 0.045 \left( \frac{f_{l,f}^{T}}{f_{c0}^{T}} \right)^{1.15} \qquad \text{for } T_{m} \ge 200 \text{ }^{\circ}\text{C}$$
(42c)

496 in which

$$\lambda_{\varepsilon} = \left[ 0.045 \left( \frac{f_{l,f}^{T}}{f_{c0}^{T}} \right)^{1.15} - 5\varepsilon_{c0T} \left( \frac{f_{l,f}^{T}}{f_{c0}^{T}} - 1 \right) \right] \left( \frac{T_{m}}{100} - 2 \right)$$
(43)

In this study, a new axial strength model was developed, applicable to FRP confined HC
columns, having a unified character with Eq. (35) when the concrete is under ambient
conditions:

$$\frac{f_{cc}^{T}}{f_{c0}^{T}} = 1 + \frac{R_{1}}{R_{2}} \left( \frac{m}{m} \frac{f_{l,f}^{T}}{f_{c0}^{T}} \right)^{R_{2}} + \frac{R_{3}}{R_{4}} \left( \frac{f_{l,f}^{T}}{f_{c0}^{T}} \right)^{R_{4}}$$
(44)

where  $R_1$ ,  $R_2$ ,  $R_3$  and  $R_4$  are the calibration factors in the determination of  $f_{cc}^T$  obtained from the regression analyses on FRP passively confined HC columns;  $\overline{m}$  is the calibration factor reflecting the influence of more expansive behavior of the concrete with a certain level of thermal damage, which activates earlier the confining system compared to the AC column at ambient temperature (based on the comparative assessment on the dilation behavior of FFCC- 505 H/FFSC-H presented in Fig. 4). In Eq. (44), the second term  $\left(\frac{R_1}{R_2}\left(\frac{m}{m}\frac{f_{l,f}^T}{f_{c0}^T}\right)^{R_2}\right)$  represents the

improvements obtained from the confinement of an AC column with axial strength equal to  $f_{c0}^{T}$ , considering the effect of earlier activation (through  $\overline{m}$ ) compared to AC; The third term (

508  $\frac{R_3}{R_4} \left( \frac{f_{l,f}^T}{f_{c0}^T} \right)^{R_4}$  ) in Eq. (44) considers the increase of confinement-induced improvements due to 509 thermal-induced damage. Based on experimental axial stress versus axial strain relations, 510 Shayanfar *et al.* [17] proposed new expressions to determine the calibration factors of  $R_1$  and 511  $R_2$ , which was rearranged by substituting  $f_{c0}$  by  $f_{c0}^T$ :

$$R_{1} = \frac{23.9}{\beta_{0T}^{0.5} \lambda_{fc} \lambda_{Rb}} \rho_{K,f}^{0.67} \le 4.25$$
(45)

$$R_2 = \frac{1.85}{\beta_{0T}^{0.2}} \rho_{K,f}^{0.26} \ge 0.3 \tag{46}$$

512 in which

$$\lambda_{fc} = 0.75 + 0.008\beta_{0T}f_{c0} \tag{47}$$

$$\lambda_{Rb} = 1.5 \left( 1 - 1.1 R_b \right) \ge 1 \tag{48}$$

where  $\lambda_{fc}$  and  $\lambda_{Rb}$  reflect the impact of concrete axial strength and the dimension of corner radius in the calibration of  $R_1$ , respectively. In order to determine the calibration factors of  $R_3$ and  $R_4$  representing the effect of thermal-induced damage in terms of confinement-induced enhancements, the experimental axial stress-strain responses reported by Bisby *et al.* [4], Lenwari *et al.* [10], Ouyang *et al.* [12] and Song *et al.* [13] were used for statistical modeling. 518 Through regression analyses on the assembled data, the calibration factors  $R_3$  and  $R_4$  are 519 determined from:

$$R_3 = \frac{\lambda_T}{\lambda_{rb}\lambda_K} \ge 0 \tag{49}$$

$$R_4 = 0.92 \left(\frac{f_{l,f}^T}{f_{c0}^T}\right)^{0.1}$$
(50)

520 in which

$$\lambda_T = 3.55 \left( \frac{T_m}{1000} \right) - 1.55 \ge 0 \tag{51}$$

$$\lambda_{K} = 1.15 - 0.022 K_{H} \frac{n_{f} t_{f} E_{f}}{D_{eq} f_{c0}}$$
(52)

$$\lambda_{th} = 1.22R_{b}^{0.25} \ge 0.85 \tag{53}$$

where  $\lambda_T$ ,  $\lambda_K$  and  $\lambda_{rb}$  reflect the impact of maximum exposure temperature ( $T_m$ ), confinement stiffness and the dimension of corner radius in the calibration of  $R_3$ , respectively. As shown in Fig. 10a, the developed model parameter ( $\lambda_T$ ) provides a sufficient agreement with the experimental counterparts, which was determined based on the best-fit relation of the proposed model with the experimental axial stress-strain responses.

526 Due to the fact that pre-existing micro-cracks in thermally damaged concrete tend to activate 527 passively confining system at the initial stage of axial compressive loading, the calibration 528 factor of  $\overline{m}$  was considered in the establishment of Eq. (44), having been obtained from 529 regression analysis to enhance the confinement effectiveness, resulting:

$$\overline{m} = 1 + m_0 \exp\left(-11.2 \frac{f_{l,f}^T}{f_{c0}^T}\right)$$
(54)

530 in which

$$m_0 = \frac{m_T}{m_\rho m_r} \tag{55}$$

$$0 \le m_T = 0.025 (T_m - 100) \le 2.5$$
 for  $T_m \le 400$  °C (56a)

$$m_T = 2.5 - 0.01 (T_m - 400) \ge 0.3$$
 for  $T_m \ge 400$  °C (56b)

$$m_r = 0.3 + 0.7R_b \tag{57}$$

$$m_{\rho} = 0.2\beta_{0T}^{0.3}\rho_{K,f}^{-0.4} \tag{58}$$

where  $m_T$ ,  $m_r$  and  $m_\rho$  are the calibration factors determined based on the regression analysis reflecting the effect of maximum exposure temperature  $(T_m)$ , corner radius ratio  $(R_b)$  and confinement stiffness  $(\rho_{K,f})$ . As shown in Fig. 10b, the developed model parameter  $(m_T)$  has a good agreement with the experimental counterparts, which extracted based on Eqs. (51 and  $\overline{m}^{Exp}$  1

535 52) 
$$(m_T^{Exp} = m_\rho m_r \frac{m^2 - 1}{\exp(-11.2f_{l,f}^T / f_{c0}^T)}$$
 where  $\overline{m}^{Exp}$  was determined using back analysis from

the best fit of the experimental results of the axial stress-strain curve of test specimens withthose obtained from the developed model).

#### 538 **5- Calculation Process**

539 In the following, the calculation methodology of the proposed model, which can be 540 implemented into a spreadsheet, for determining the axial response of FRP confined concrete 541 submitted to a certain level of thermal damage is presented. The calculation procedure is as:

542 **1.** Determine the mechanical characteristics of unconfined heat-damaged concrete:

- Peak axial strength  $(f_{c0}^T)$  by Eq. (1)

544 - Axial strain corresponding to  $f_{c0}^{T}$  ( $\varepsilon_{c0}^{T}$ ) by Eq. (6)

545 **2.** Assume a value for  $\varepsilon_c$  on the interval  $(0, \varepsilon_{cu}]$  where  $\varepsilon_{cu}$  is the ultimate axial strain when 546 FRP rupture occurs.

- 547 **3.** Determine the dilation response corresponding to  $\varepsilon_c$
- 548 Secant Poisson's ratio  $(v_s^T)$  by Eq. (29) and the data presented in Fig. 6
- 549 Confinement pressure  $(f_{l,f}^T)$  by Eq. (22)
- 550 **4.** Determine the axial response corresponding to  $\mathcal{E}_c$
- Calibration factors  $R_1$ ,  $R_2$ ,  $R_3$  and  $R_4$ , by Eqs. (45), (46), (49), and (50)
- 552  $\overline{m}$  factor from Eq. (54)
- 553 Peak axial strength  $(f_{cc}^T)$  by Eq. (44)
- Axial strain  $(\varepsilon_{cc}^{T})$  corresponding to  $f_{cc}^{T}$  by Eq. (42)
- 555 Axial stress  $(f_c^T)$  by Eq. (39)

556 **5.** Continue the aforementioned incremental procedure up to  $\varepsilon_{cu}$ ,  $f_c^T$  versus  $\varepsilon_c$  relation can 557 be calculated.

558

Since the focus of the current study was given on the simulation of global axial stress-strain curves, the experimental values of ultimate axial strain ( $\varepsilon_{cu}$ ) was used to terminate the computation process.

562 It is noteworthy that the reliability of regression analyses performed for developing predictive

563 equations (as key components of the proposed model) is limited to the range of input/output

- variables supported in the used database. Accordingly, the predictive performance of these
- sequations can be improved through recalibrating the model components based on new datasets
- 566 consisting of the relevant variables with a broader range. Furthermore, the experimental data

567	used for calibrating the failure surface function and the coupled dilation model was obtained
568	from tests on relatively small FRP confined prototypes of square/circular concrete specimens
569	where thermal distribution inside the concrete can be reasonably considered uniform.
570	Therefore, for real cases with a larger dimension and non-uniform thermal distribution whose
571	relative variables might not be in the aforementioned interval, the key components of the
572	proposed model might need to be recalibrated, which will be the focus of a future study.
573	Considering the relatively simple methodology of the proposed analytical-based model, it can
574	be extended potentially to FRP confined heat-damaged RC columns of rectangular cross-
575	section, through addressing properly the influences of dual FRP-steel confinement, sectional
576	aspect ratio (the ratio of longer and shorter cross-section dimensions) and their interactions
577	with exposure temperature in terms of axial and dilation behavior.

### 578 **6- Verification**

This section assesses the predictive performance of the developed analysis-oriented model for the prediction of axial response of concrete specimens submitted to a certain maximum exposure temperature, and after the specimens have attained the environmental temperature, subsequently, confined with FRP confining system. For this purpose, the axial stress-strain curve obtained from the proposed model is compared to that obtained from the experimental studies conducted by Bisby *et al.* [4], Lenwari *et al.* [10], Ouyang *et al.* [12] and Song *et al.* [13].

Bisby *et al.* [4] performed an experimental study to investigate the axial stress-strain response
of FRP fully confined circular HC columns. The diameter and height of the test specimens

588 were 100 mm and 200 mm, respectively. The axial compressive strength of AC column at the room temperature was 28 MPa. The values of nominal thickness, modulus of elasticity and 589 rupture strain of CFRP jackets were reported as 0.12 mm, 241.1 GPa and 1.7%, respectively. 590 591 All the specimens submitted to a certain level of maximum exposure temperature were confined by one CFRP layer. Complete details regarding the test specimens can be found from 592 Bisby et al. [4]. Fig. 11 presents the comparison of the results obtained from the analytical 593 594 model with those measured experimentally. As can be seen, the model has a good predictive performance in the estimation of axial responses of the test specimens submitted to 300 °C, 595 500 °C and 700 °C, even though there is a slight overestimation in terms of maximum axial 596 strength for T500-L1. 597

Lenwari et al. [10] experimentally determined the axial stress-strain response of FRP fully 598 confined circular HC columns. The diameter and height of the test specimens were 150 mm 599 and 300 mm, respectively. The axial compressive strength of AC column at the room 600 temperature was 40.5 MPa. The values of nominal thickness, modulus of elasticity and rupture 601 strain of CFRP jackets were reported as 0.131 mm, 234.1 GPa and 1.8%, respectively. All the 602 603 specimens submitted to a certain level of maximum exposure temperature were confined by 604 one CFRP layer. Complete details regarding the test specimens can be found from Lenwari et al. [10]. Fig. 12 demonstrates the comparison of the results obtained from the analytical model 605 with those measured experimentally. As can be seen, the model was able to predict the 606 607 experimental counterparts with a good agreement, even though there is a slight overestimation in terms of maximum axial strength for T300-L1 and T500-L1. 608

For further investigation of the capability of the developed confinement model, the axial stressstrain curves obtained from experimental studies conducted by Ouyang *et al.* [12] and Song *et al.* [13], where the test specimens were submitted to a high level of thermal-induced damage (

612  $T_m \ge 600 \text{ °C}$ ), are compared with those analytically obtained from the model, as shown in Figs. 613 13 and 14. As can be observed, the model could accurately predict the full range of the 614 experimentally measured axial responses, except for a slight underestimation for the cases of 615 T600-L3 and T600-L3 tested by Song *et al.* [13] (Figs. 14e and f).

Due to the unified character of the proposed analysis-oriented model at ambient and elevated 616 temperature conditions, Fig. 15 compares the axial stress- strain relations of FFSC-A reported 617 from the experimental study conducted by Wang and Wu [6] with those analytically obtained 618 from the model to assess its capability for the cases at ambient condition. All specimens had a 619 section dimension of 150 mm and a height of 300 mm, with a sectional corner radius ratio ( $R_{\rm h}$ 620 ) varying from 0 (r = 0) to 1 (r = 75 mm) representing a square cross section with sharp edges 621 and circular cross-section, respectively. Two series of FFSC-A specimens with concrete 622 strengths of  $f_{c0} \simeq 30$  MPa and  $f_{c0} \simeq 50$  MPa were tested. The CFRP thickness, tensile elastic 623 624 modulus and rupture strain were 0.165 mm, 219 GPa, and 1.99%, obtained from flat coupon tensile tests. The complete details of the experimental program can be found in Wang and Wu 625 [6]. As can be seen in Fig. 15, in general, there are a good agreement between the experimental 626 axial stress-strain relationships with those obtained from the proposed model, confirming the 627 successful simulation of the corner radius ratio  $(R_{h})$  influence on confinement-induced 628 629 enhancements of FFSC-A at ambient conditions.

# 630 7- Summary and Conclusion

This paper has addressed the development of a new analysis-oriented model to predict the axial and dilation behavior of FRP confined HC circular/square concrete columns. Through regression analyses performed on a large database of unconfined heat-damaged concrete experimentally tested specimens, new expressions were developed to determine its mechanical

635	characteristics in terms of axial compressive strength and its corresponding axial strain. A new
636	model was developed to determine dilation response of FRP confined HC columns by
637	formulating the effect of thermal damage level on Poisson's coefficient versus axial strain
638	relationship. Subsequently, a new axial stress-strain model, coupled with the developed dilation
639	model, was proposed to calculate the axial behavior of FRP confined HC columns with the
640	different levels of maximum exposure temperature. Comparisons with axial and dilation results
641	reported by available experiment studies in the literature verified that the developed analysis-
642	oriented model is able to predict the experimental counterparts with good accuracy, and has a
643	relatively simple format for design purposes by using a data sheet.
644	
645	
646	
647	
648	
649	
650	
651	

# 652 Data Availability Statement

653	All data and models related to the present study could be available from the corresponding
654	author upon rational request.
655	
656	
657	
658	
659	Acknowledgments
660	This study is a part of the project "StreColesf_Innovative technique using effectively composite
661	materials for the strengthening of rectangular cross-section reinforced concrete columns
662	exposed to seismic loadings and fire", with the reference POCI-01-0145-FEDER-029485. The
663	firs author also acknowledges the support provided by FCT PhD individual fellowship 2019
664	with the reference of "SFRH/BD/148002/2019".
665	
666	
667	
668	
669	
670	
671	
672	
673	
674	

## 675 **References**

- Kodur, V. (2014). Properties of concrete at elevated temperatures. International Scholarly
   Research Notices.
- Bamonte, P., & Lo Monte, F. (2015). Reinforced concrete columns exposed to standard fire:
   Comparison among different constitutive models for concrete at high temperature. Fire safety
   journal, 71, 310-323.
- 681
  3. Demir, U., Green, M. F., & Ilki, A. (2020). Postfire seismic performance of reinforced precast concrete columns. PCI Journal, 65(6).
- 683 4. Bisby, L. A., Chen, J. F., Li, S. Q., Stratford, T. J., Cueva, N., & Crossling, K. (2011).
  684 Strengthening fire-damaged concrete by confinement with fibre-reinforced polymer wraps.
  685 Engineering Structures, 33(12), 3381-3391.
- 5. Barros JA, Ferreira DR. Assessing the efficiency of CFRP discrete confinement systems for concrete cylinders. J Compos Constr 2008;12(2):134-148.
- 688 6. Wang LM, Wu YF. Effect of corner radius on the performance of CFRP-confined square
  689 concrete columns: test. Eng Struct 2008;30:493–505.
- For a strengthening technique for increasing
  Janwaen, W., Barros, J. A., & Costa, I. G. (2019). A new strengthening technique for increasing
  the load carrying capacity of rectangular reinforced concrete columns subjected to axial
  compressive loading. Composites Part B: Engineering, 158, 67-81.
- 8. Shayanfar J, Rezazadeh M, Barros JA (2020a). Analytical model to predict dilation behavior
  of FRP confined circular concrete columns subjected to axial compressive loading. J Compos
  Constr 2020;24(6):04020071.
- 696 9. Shan B, Gui FC, Monti G, Xiao Y (2019). Effectiveness of CFRP confinement and compressive
  697 strength of square concrete columns. J Compos Constr 2019 23(6):04019043
- Lenwari, A., Rungamornrat, J., & Woonprasert, S. (2016). Axial compression behavior of firedamaged concrete cylinders confined with CFRP sheets. Journal of Composites for
  Construction, 20(5), 04016027.
- 11. Luo, X., Sun, W., & Chan, S. Y. N. (2000). Effect of heating and cooling regimes on residual
  strength and microstructure of normal strength and high-performance concrete. Cement and
  Concrete Research, 30(3), 379-383.
- 704 12. Ouyang, L. J., Chai, M. X., Song, J., Hu, L. L., & Gao, W. Y. (2021). Repair of thermally
  705 damaged concrete cylinders with basalt fiber-reinforced polymer jackets. Journal of Building
  706 Engineering, 44, 102673.
- 13. Song, J., Gao, W. Y., Ouyang, L. J., Zeng, J. J., Yang, J., & Liu, W. D. (2021). Compressive
  behavior of heat-damaged square concrete prisms confined with basalt fiber-reinforced polymer
  jackets. Engineering Structures, 242, 112504.
- Teng J, Huang YL, Lam L, Ye LP. Theoretical model for fiber-reinforced polymer-confined
   concrete. J Compos Constr 2007;11(2):201-210.

- 15. Lim JC, Ozbakkaloglu T (2014a). Unified stress-strain model for FRP and actively confined
   normal strength and high-strength concrete. J Compos Constr 2014;19(4):04014072.
- Shayanfar, J., Barros, J. A., & Rezazadeh, M. (2021a). Generalized Analysis-oriented model of
   FRP confined concrete circular columns. Composite Structures, 270, 114026.
- 716 17. Shayanfar, J., Barros, J. A., & Rezazadeh, M. (2022). Unified model for fully and partially FRP
  717 confined circular and square concrete columns subjected to axial compression. Engineering
  718 Structures, 251, 113355.
- 18. Kodur, V. K. R., & Sultan, M. A. (2003). Effect of temperature on thermal properties of high strength concrete. Journal of materials in civil engineering, 15(2), 101-107.
- 19. Hertz, K. D. (2005). Concrete strength for fire safety design. Magazine of concrete research,
  57(8), 445-453.
- 20. Raut, N. K., & Kodur, V. K. R. (2011). Response of high-strength concrete columns under design fire exposure. Journal of Structural Engineering, 137(1), 69-79.
- Aslani, F., & Bastami, M. (2011). Constitutive relationships for normal-and high-strength
  concrete at elevated temperatures. ACI Materials Journal, 108(4), 355.
- 727 22. Chang, Y.F., Chen, Y.H., Sheu, M.S., and Yao, G.C. (2006). "Residual stress-strain
  728 relationship for concrete after exposure to high temperatures." Cement and Concrete Research,
  729 36, 1999–2005.
- Al-Salloum, Y. A., Elsanadedy, H. M., & Abadel, A. A. (2011). Behavior of FRP-confined
  concrete after high temperature exposure. Construction and Building Materials, 25(2), 838-850.
- 732 24. Sharma, U., Zaidi, K., & Bhandari, N. (2012). Residual compressive stress-strain relationship
   733 for concrete subjected to elevated temperatures. Journal of Structural Fire Engineering.
- 734 25. Geng, J., Sun, Q., Zhang, W., & Lü, C. (2016). Effect of high temperature on mechanical and
  735 acoustic emission properties of calcareous-aggregate concrete. Applied Thermal Engineering,
  736 106, 1200-1208.
- 737 26. Xiao, J., Li, Z., Xie, Q., & Shen, L. (2016). Effect of strain rate on compressive behaviour of
  738 high-strength concrete after exposure to elevated temperatures. Fire Safety Journal, 83, 25-37.
- 739 27. Xiang, S., Zeng, L., Zhang, J., Chen, J., Liu, Y., Cheng, G., & Mo, J. (2019). A DIC-based
  740 study on compressive responses of concrete after exposure to elevated temperatures. Materials,
  741 12(13), 2044.
- 28. Li, L. Y., & Purkiss, J. (2005). Stress-strain constitutive equations of concrete material at
  elevated temperatures. Fire Safety Journal, 40(7), 669-686.
- 744 29. Han, L. H., & Huo, J. S. (2003). Concrete-filled hollow structural steel columns after exposure
  745 to ISO-834 fire standard. Journal of Structural Engineering, 129(1), 68-78.
- 746 30. Eurocode 2: Design of Concrete Structures ENV EC2. 1992.
- 747 31. Lie, T. T., & Lin, T. D. (1985). Fire performance of reinforced concrete columns. In: ASTM
  748 STP 882. Fire Safety: Science and Engineering. p. 176–205.

749 32. Lie, T. T., Rowe, T. J., & Lin, T. D. (1986). Residual strength of fire-exposed reinforced concrete columns. Detroit: American Concrete Institute; Special Publication, 92, 153-174. 750 33. Dahl, K. K. B. (1992). "Uniaxial stress-strain curves for normal and highstrength concrete." 751 ABK Rep. No. R282, Dept. of Structural Engineering, Technical Univ. of Denmark, Kongens 752 Lyngby, Denmark. Eurocode 2: Design of Concrete Structures ENV EC2. 1992. 753 754 34. Jansen, D. C., & Shah, S. P. (1997). Effect of length on compressive strain softening of concrete. Journal of engineering mechanics, 123(1), 25-35. 755 35. Watanabe, K., Niwa, J., Yokota, H., and Iwanami, M. (2004). "Experimental study on stress-756 757 strain curve of concrete considering localized failure in compression." J. Adv. Concr. Technol., 2(3), 395–407. 758 759 36. Wei, Y., & Wu, Y. F. (2016). Experimental study of concrete columns with localized failure. 760 Journal of Composites for Construction, 20(5), 04016032. 761 37. Wu YF, Wei Y (2016). Stress-Strain Modeling of Concrete Columns with Localized Failure: 762 An Analytical Study. J Compos Constr 2016;20(3):04015071. 763 38. Yang, K. H., Lee, Y., & Mun, J. H. (2019). A Stress-Strain Model for Unconfined Concrete in Compression considering the Size Effect. Advances in Materials Science and Engineering, 764 765 2019. 39. Popovics S. A numerical approach to the complete stress-strain curve of concrete. Cement and 766 concrete research 1973;3(5):583-599. 767 40. Karthik MM, Mander JB. Stress-block parameters for unconfined and confined concrete based 768 on a unified stress-strain model. J Struct Eng 2010;137(2):270-273. 769 770 41. Lim JC, Ozbakkaloglu T (2014b). Stress-strain model for normal-and light-weight concretes under uniaxial and triaxial compression. Constr Build Mater 2014;71:492-509. 771 42. Terro, M. J., 1998, "Numerical Modeling of the Behavior of Concrete Structures in Fire," ACI 772 773 Structural Journal, V. 95, No. 2, Mar.-Apr., pp. 183-193. 43. Khennane A, Baker G. Uniaxial model for concrete under variable temperature and stress. J 774 775 Eng Mech-ASCE 1993;119(8):1507-25. 776 44. Bazant P, Chern JC. Stress-induced thermal and shrinkage strains in concrete. J Eng Mech-ASCE 1987;113(10):1493-511. 777 45. Lie TT. Structural fire protection. New York: American Society of Civil Engineers; 1992. 778 779 46. Mirmiran A, Shahawy M. Dilation characteristics of confined concrete. Mechanics of 780 Cohesive- frictional Materials: Mech Cohesive-Frict Mater 1997;2(3):237-249. 47. Lim JC, Ozbakkaloglu T (2014c). Hoop strains in FRP-confined concrete columns: 781 782 experimental observations. Mater Struct 2014;48(9):2839-2854. 783 48. Zeng, J.-J., Guo, Y.-C., Gao, W.-Y., Li, J.-Z., and Xie, J.-H. (2017). "Behavior of partially and fully FRP confined circularized square columns under axial compression." Construction and 784 785 Building Materials, 152, 319-332.

- 49. Shayanfar J, Rezazadeh M, Barros JA, Ramezansefat H (2020b). A new dilation model for FRP fully/partially confined concrete column under axial loading. The 3RD RILEM Spring Convention 2020 Ambitioning a Sustainable Future for Built Environment: Comprehensive Strategies for Unprecedented Challenges, Guimarães Portugal 2020.
- 50. Lertsrisakulrat, T., Watanabe, K., Matsuo, M., and Niwa, J. (2001). "Experimental study on parameters in localization of concrete subjected to compression." J. Mater. Concr. Struct.
  Pavement, 669(50), 309–321.
- 51. Candappa DC, Sanjayan JG, Setunge S. Complete triaxial stress-strain curves of high-strength concrete. Journal of Materials in Civil Engineering 2001;13(3):209-215.
- 52. Shayanfar, J., Rezazadeh, M., & Barros, J. A. (2021b). Theoretical Prediction of Axial
  Response of FRP Fully/partially Confined Circular Concrete Under Axial Loading. In
  International Conference on Fibre-Reinforced Polymer (FRP) Composites in Civil Engineering
  (pp. 1439-1449). Springer, Cham.
- 53. Lin, G., & Teng, J. G. (2020). Advanced stress-strain model for FRP-confined concrete in
  square columns. Composites Part B: Engineering, 197, 108149.
- 54. Yang, J., Wang, J., & Wang, Z. (2020). Axial compressive behavior of partially CFRP confined
  seawater sea-sand concrete in circular columns–Part II: A new analysis-oriented
  model. *Composite Structures*, 246, 112368.
- Solution Solution

# **1** Stress–strain Model for FRP Confined Heat-damaged Concrete Columns

2

Javad Shayanfar<sup>1</sup>, Joaquim A. O. Barros<sup>2</sup> and Mohammadali Rezazadeh<sup>3</sup>

<sup>1</sup> PhD Candidate, ISISE, Department of Civil Engineering, University of Minho, Azurém 4800-058 Guimarães, Portugal, <u>arch3d.ir@gmail.com</u> (corresponding author)

<sup>2</sup> Full Prof., ISISE, IBS, Department of Civil Engineering, University of Minho, Azurém 4800-058 Guimarães, Portugal, <u>barros@civil.uminho.pt</u>

<sup>3</sup> Lecturer, Civil Eng., Department of Mechanical and Construction Engineering, Northumbria University, Newcastle upon Tyne, NE1 8ST, United Kingdom, <u>mohammadali.rezazadeh@northumbria.ac.uk</u>

3

#### 4 Abstract:

5 This paper is dedicated to the development of a new analysis-oriented model to simulate the axial and 6 dilation behavior of FRP confined heat-damaged concrete columns under axial compressive loading. 7 The model's calibration has considered the experimental results from concrete circular/square cross-8 section specimens submitted to a certain level of heat-induced damage, which after attained the 9 environmental temperature, were fully confined with FRP jacket and tested. New equations were 10 developed to determine the mechanical characteristics of unconfined heat-damaged concrete by 11 performing regression analysis on a large database of experimental tests. Based on a parametric study 12 on dilation behavior of FRP confined heat-damaged columns, a new dilation model was developed to 13 predict concrete lateral strain at a given axial strain, dependent on the thermal damage level. By using 14 this dilation model, a new methodology was introduced for predicting the axial stress-strain response 15 of FRP confined heat-damaged columns in compliance with the active confinement approach. The 16 adequate predictive performance of the model is demonstrated by estimating experimental axial stress-17 strain results.

18 Keywords: FRP confined heat-damaged concrete; thermal damage; confinement model; dilation
19 behavior

20

#### 21 **1- Introduction**

During fire, concrete buildings generally demonstrate a better fire performance compared to 22 timber and steel buildings due to concrete non-combustibility and relatively low thermal 23 conductivity (Kodur [1], Bamonte and Lo Monte [2]). Nonetheless, depending on the fire 24 intensity imposed to the structural elements, material deteriorations occur during fire exposure, 25 resulting detrimental effects on the performance of concrete structures at their serviceability 26 and ultimate limit state conditions (Demir et al. [3]). Considering the pre-existing thermal-27 induced damage, a post-fire strengthening solution for restoring its structural performance can 28 be an environmental and economic sustainable solution over the demolishing and rebuilding 29 30 alternative. To reinstate sufficiently axial responses of heat-damaged concrete columns (HC), 31 externally bonded fiber-reinforced-polymer (FRP) composites have been demonstrated as a viable solution (Bisby et al. [4]). 32

33 Several experimental and analytical studies (i.e. Barros and Ferreira [5], Wang and Wu [6], Janwaen et al. [7], Shayanfar et al. [8]) were conducted to evaluate the capability of FRP 34 confining strategy in upgrading the axial and dilation behavior of FRP confined concrete 35 columns under axial compression at ambient conditions. For the case of FRP fully confined 36 concrete columns of circular cross section at ambient conditions (FFCC-A, as shown in Fig. 37 1a), Barros and Ferreira [5] experimentally evidenced that the confinement-induced 38 39 enhancements for normal-strength concrete is more pronounced than those registered in high-40 strength concrete. For the case of FRP fully confined concrete columns of square cross section at ambient conditions (FFSC-A, as shown in Fig. 1a), Wang and Wu [6] and Shan et al. [9] 41 conducted experimental studies to evaluate the influence of cross-section circularity in the 42 effectiveness of the confining strategy. It was evidenced that decreasing the corner radius (r)43 from r = b/2 (circular columns where b defines the length of the cross-section dimension) to r 44

45 = 0 (square columns with sharp edges) results in a significant reduction in terms of confinement
46 efficiency.

47 On the other hand, very limited experimental studies have been conducted for assessing the strengthening efficiency of FRP confining systems applied in the post-cooling regime of 48 49 concrete specimens subjected to a certain maximum exposure temperature according to the 50 heating scheme demonstrated in Fig. 1b. Bisby et al. [4] performed an experimental research 51 to assess the effectiveness of FRP fully confinement on circular concrete columns subjected to 52 different levels of maximum temperature (300, 500 and 700 °C) (FFCC-H, as shown in Fig. 53 1a). It was evidenced that FRP confinement could significantly increase the axial compressive strength and stiffness of unconfined heat-damaged specimens (Fig. 1c). The peak axial 54 compressive strength and the corresponding axial strain of FFCC-H specimens subjected to 55 severe thermal exposure (700 °C) were almost 90% and 145%, respectively, of those of FFCC 56 at ambient conditions. However, the secant axial stiffness of FFCC-H specimens (as the ratio 57 58 of axial stress to its corresponding axial strain) was reported to be considerably lower than that of FFCC, and this difference has increased with maximum exposure temperature  $(T_m)$ . Lenwari 59 et al. [10] experimentally evidenced that the axial stress versus axial strain response of FFCC-60 H is dependent on the used heating scheme, i.e.  $T_m$ , exposure duration and cooling regime (air 61 or water cooling methods), and on the axial compressive strength of AC, which was also 62 confirmed by Luo et al. [11]. Furthermore, it was shown that the level of axial strength 63 improvements, induced by FRP confining system, is higher in HC than in AC. Accordingly, 64 for HC with a high level of thermal damage, FRP effectiveness tends to be more significant. 65 66 Ouyang et al. [12] investigated experimentally the dilation behavior of heat-damaged circular concrete specimens confined by Basalt FRP (BFRP) jacket (FFCC-H) under axial compressive 67 loading. It was demonstrated that there is a noticeable difference between the transverse 68 expansibility of HC subjected to different level of the imposed  $T_m$ . Furthermore, the recorded 69

hoop strains at BFRP rupture were almost independent of the exposure temperature. Song *et al.* [13] experimentally evidenced the high potential of BFRP confining system for improving
the axial and dilation responses of HC with square cross-section (FFSC-H, as shown in Fig.
1a). The confinement-induced enhancements were more pronounced in HC exposed to high
temperatures and confined by thicker BFRP jackets.

75 For the prediction of the axial stress-strain response of FRP confined AC columns, several 76 analysis-oriented models, based on active confinement approach, have been recommended i.e. 77 Teng et al. [14], Lim and Ozbakkaloglu [15], and Shayanfar et al. [16 and 17]. Teng et al. [14] 78 proposed an analysis-oriented model for passively confined concrete, whose calibration was based on experimental observations in FRP fully confined concrete specimens of circular cross 79 section (FFCC). Based on theoretical principles and experimental evidences, Shayanfar et al. 80 [16] developed a generalized analysis-oriented model for passive confinement arrangements, 81 whose parameters were derived from the experimental results with FRP fully/partially confined 82 83 circular concrete specimens. Shayanfar et al. [17] extended Shayanfar et al. [16]'s model to make it applicable to the case of columns of square-cross section, by simulating the influence 84 of the non-circularity in terms of confinement-induced enhancements. Bisby *et al.* [4] proposed 85 86 a design-oriented model to determine the axial response of heat-damaged circular cross-section concrete columns confined by FRP (FFCC-H). In this model, the confinement-induced 87 improvements were expressed as a main function of maximum exposure temperature  $(T_m)$ 88 imposed to the column. Nevertheless, an analysis-oriented model to simulate the full-range of 89 dilation and axial responses of FRP fully confined HC columns with square cross-section is 90 91 still lacking.

92 This paper aims to introduce a new methodology to determine the axial stress-strain response
93 of FRP fully confined circular/square HC columns (the concrete specimens were submitted to

94 a certain  $T_m$ , and after having attained the environmental temperature, the fully confining FRP jacket was applied to the heat-damaged concrete). For the case of unconfined heat-damaged 95 concrete, through regression analysis performed on a large test database, new expressions are 96 97 developed to determine its mechanical characteristics in terms of axial compressive strength and its corresponding axial strain. By performing parametric studies with the available 98 experimental data, the significant influence of the pre-existing thermal-induced damage on the 99 100 establishment of the axial and dilation behavior of FRP fully confined heat-damaged concrete columns is demonstrated. By performing a parametric study to assess the influence of  $T_m$  on 101 102 the concrete transverse expansion, a new dilation model depending on the heat-damaged level is proposed, which has a unified character with the dilation model developed by Shayanfar et 103 104 al. [17] for concrete specimens at room temperature. By using the developed dilation model, a 105 new methodology is introduced, based on active confinement approach, for the simulation of 106 the axial stress-strain response of FRP fully confined circular/square HC columns at the different levels of  $T_m$ . The model's adequate predictive performance is demonstrated by 107 estimating experimental axial stress-strain responses. 108

109 2- Unconfined heat-damaged concrete columns (HC)

Kodur [1] evidenced that post-fire response of HC columns significantly depends on concrete 110 mechanical, thermal (including thermal conductivity, thermal diffusivity, specific heat, and 111 112 mass loss) and deformation (including concrete thermal expansion) properties, as well as on the spalling response. In general, concrete submitted to maximum exposure temperature  $(T_m)$ 113 up to 100 °C can be considered almost undamaged. Afterward, water loss (causing shrinkage) 114 and the expansion of aggregates induce internal stresses in the concrete, particularly for 115  $T_m \ge 300$  °C. Furthermore, thermal-induced chemical processes and thermo-mechanical 116 damages lead to a significant strength degradation for the concrete submitted to high levels of 117

exposure temperature [1]. A comprehensive review of concrete properties at elevated
temperatures can be found in Kodur and Sultan [18], Hertz [19], Raut and Kodur [20], Aslani
and Bastami [21].

In terms of mechanical properties, by submitting concrete to elevated temperature with a heating scheme including maximum exposure temperature  $(T_m)$ , the axial compressive stress of HC  $(f_c^T)$  and the modulus of elasticity  $(E_{cT})$  decrease depending upon its peak axial strength  $(f_{c0}^T)$ . However, axial strains corresponding to the peak  $(\varepsilon_{c0}^T)$  and ultimate stages  $(\varepsilon_{cu0}^T)$ increase, demonstrating a significant reduction on the axial stiffness (defined as  $f_c^T / \varepsilon_c$  where  $\varepsilon_c$  is the axial strain) of HC compared to AC (Hertz [19], Chang *et al.* [22], Al-Salloum *et al.* [23], Sharma *et al.* [24], Geng *et al.* [25], Xiao *et al.* [26], Xiang *et al.* [27]).

# 128 **2-1- Peak axial strength of HC** $(f_{c0}^T)$

Experimental studies evidenced that the heat-induced damages in HC columns lead to a reduction in terms of peak axial strength. Accordingly, by defining the axial strength ratio,  $\beta_{0T}$ , (the ratio of  $f_{c0}^{T}$  and  $f_{c0}$ ),  $f_{c0}^{T}$  can be expressed as:

$$f_{c0}^{T} = \beta_{0T} f_{c0} \tag{1}$$

The variation of  $\beta_{0T}^{Exp} = f_{c0}^{T} Exp / f_{c0}^{Exp}$  with respect to  $T_m$  can be obtained from experimental results of axial compression tests on HC columns. In the present study, a database of 292 HC column specimens with a wide range of concrete properties and exposure temperature was collected, as briefly presented in Table 1. The following criteria were adopted to include/exclude experimental data: 1) ones obtained from circular/square/rectangular heatdamaged concrete specimens tested under concentric were included; 2) heat-damaged concrete specimens subjected to a maximum exposure temperature more than 800 °C were excluded; 3)

Fig. 2a shows the variation of 
$$\beta_{0T}^{Exp}$$
 with respect to  $T_m$ , based on the results of the database,  
where a decrease of  $\beta_{0T}^{Exp}$  with the increase of  $T_m$ , from 1 to almost 0.2 corresponding to room  
conditions and 800 °C, respectively, is visible. Based on the best-fit relation obtained from  
fregression analysis on the database information,  $\beta_{0T}$  versus  $T_m$  data can be obtained as  
 $\beta_{0T} = 1.087 - 0.00116T_m$ . By assuming *Error Index* as  $(1.087 - 0.00116T_m)/\beta_{0T}^{Exp}$ , Fig. 2b  
demonstrates that there is a slight variation in Error Index versus concrete strength relationship  
which is less than one up to almost  $f_{c0} = 110$  MPa, representing underestimation. However,  
beyond  $f_{c0} = 110$  MPa, the Error Index tend to be more than 1 resulting in overestimation of  
the experimental counterparts. Accordingly, based on regression analysis performed on the  
Error Index and concrete strength relationship,  $\beta_{0T}$  can be calculated by:

$$\beta_{0T} = \frac{1.087 - 0.00116T_m}{\gamma_f} \le 1$$
<sup>(2)</sup>

153 in which

$$\gamma_f = 1 + (\gamma_0 - 1) \left( \frac{T_m - 25}{100} \right)$$
 for  $T_m \le 100 \text{ °C}$  (3a)

$$\gamma_f = \gamma_0 \qquad \qquad \text{for } T_m \ge 100 \text{ °C}$$
(3b)

$$\gamma_0 = 3415 \left(\frac{f_{c0}}{1000}\right)^3 - 721 \left(\frac{f_{c0}}{1000}\right)^2 + 44.5 \left(\frac{f_{c0}}{1000}\right) + 0.178$$
(4)

where the developed expression is valid for  $T_m \leq 800$  °C based on the interval of the submitted maximum exposure temperatures ( $T_m = [25 \text{ °C}, 800 \text{ °C}]$ ) in the database used for the regression analysis.  $\gamma_0$  reflects the influence of  $f_{c0}$  (in MPa) in the determination of  $\beta_{0T}$ empirically.

In Fig. 2c, the results predicted by the proposed model are compared to those reported by the experiments (Table 2), with a mean = 0.964, a coefficient of variation (CoV) = 0.279, a mean absolute percentage error (MAPE) = 0.203, and an R-squared value ( $R^2$ ) = 0.876, revealing an acceptable predictive performance. Table 2 also shows that the proposed model provides a predictive performance better than of the existing models.

# 163 **2-2-** Axial strain at the peak stage of AC columns ( $\varepsilon_{c0}$ )

For the case of AC columns, the experimental and analytical studies conducted by [33-38] 164 evidenced that  $\varepsilon_{c0}$  increases with the concrete compressive strength ( $f_{c0}$ ). Jansen and Shah 165 [34] experimentally demonstrated that the column aspect ratio ( $\lambda_L$  as the ratio of the column 166 height to its diameter) has also considerable influence on  $\varepsilon_{c0}$  due to the occurrence of strain-167 localization within a finite zone with a pronounced gradient of deformations due to the concrete 168 post-peak strain-softening behavior. In this study, in order to estimate  $\varepsilon_{c0}$ , a large database 169 (Table 3) was compiled from the experimental results available in the literature, resulting in 170 604 unconfined concrete specimens (AC) with a broad range of concrete properties and 171 geometry configurations. Note that for the case of non-circular columns with a total cross-172 section area of  $A_g$ , based on Yang *et al.* [38] recommendations,  $\lambda_L$  can be determined as  $L/d_{eq}$ 173

where *L* is the columns' height and  $d_{eq}$  is the equivalent circular diameter ( $d_{eq} = \sqrt{4A_g/\pi}$ [38]).

Based on a preliminary sensitivity analysis, a low effect was achieved for the influence of the column size (i.e. the normalized  $d_{eq}/150$ , with  $d_{eq}$  in mm) to estimate  $\varepsilon_{c0}$  when compared to other influencing factors ( $f_{c0}$  and  $\lambda_L$ ). Accordingly, using regression analysis, the best-fit expression to predict  $\varepsilon_{c0}$  was derived as a function of  $f_{c0}$  and  $\lambda_L$  regardless of the column's cross-section dimension influence:

$$\varepsilon_{c0} = 0.0011 \left(\frac{f_{c0}}{\lambda_L}\right)^{0.25}$$
(5)

Table 4 evaluates the predictive performance of this relation with the results of the experimental tests, and also compares with that of existing models. Based on the assessment indicators (values of mean = 0.977, CoV = 0.184 and MAPE = 0.138), there is an acceptable agreement between model prediction and the experimental results. Furthermore, compared to the models recommended by Popovics [39], Karthik and Mander [40] and Lim and Ozbakkaloglu [41], it is the most accurate one, confirming its reliability.

# 187 **2-3-** Axial strain at the peak stage of HC columns ( $\varepsilon_{c0}^{T}$ )

The experiments with HC columns conducted by Chang *et al.* [22], Sharma *et al.* [24], Xiao *et al.* [26], Xiang *et al.* [27] evidenced that the axial strain  $(\varepsilon_{c0}^{T})$  corresponding to  $f_{c0}^{T}$  tends to increase significantly from  $\varepsilon_{c0}$  at ambient condition to  $\varepsilon_{c0}^{T} \gg \varepsilon_{c0}$  at elevated temperature, as shown in Fig. 3a.

The details of the experimental specimens in the assembled database, including 225 tested HCcolumns, is presented in Table 5.

194 The best-fit relation between  $\varepsilon_{c0}^{T Exp} / \varepsilon_{c0} - 1$  (representing the thermal damage-induced strain) 195 and  $T_m$  was obtained from regression analysis by considering the influence of  $f_{c0}$ , resulting:

$$\varepsilon_{c0}^{T} = \left(1 + 63f_{c0}^{-0.5} \left(\frac{T_{m}}{1000}\right)^{4.2}\right) \frac{\varepsilon_{c0}}{\alpha_{T}} \le 4.5 \frac{\varepsilon_{c0}}{\alpha_{T}}$$
(6)

in which

 $\alpha_T = 1 \qquad \qquad \text{for } T_m \le 100 \text{ °C} \tag{7a}$ 

$$\alpha_T = 1.22 - 0.0025T_m + 3 \times 10^{-6} T_m^2 \qquad \text{for } T_m > 100 \text{ }^{\circ}\text{C} \tag{7b}$$

where the developed expression is valid for  $T_m \leq 800$  °C based on the interval of the submitted 197 maximum exposure temperatures  $(T_m = [25 \text{ °C}, 800 \text{ °C}])$  in the database used for the 198 regression analysis.  $\alpha_T$  is the calibration factor for the influence of  $T_m$  in the increase of axial 199 strain induced by thermal damage, obtained from the regression analysis. In Fig. 3b and Table 200 6, the predictive performance of this model is assessed based on 225 test specimen results. As 201 can be seen, Eq. (6) provides the most accurate model compared to the existing models in the 202 prediction of the experimental counterparts, even though conservative results were achieved 203 204 for some cases submitted to high level of exposure temperature.

### 205 3-Dilation behavior of FRP confined HC columns

### 206 **3-1-** Confinement pressure developed for ambient condition

207 For the case of FRP fully confined square AC columns (FFSC), based on the force equilibrium

at the cross-sectional level, confinement pressure  $(f_{l,f})$  generated by the FRP confining stress

209 ( $f_f$ ) can be expressed as (Shayanfar *et al.* [17]):

$$f_{l,f} = 2K_e \frac{n_f t_f}{D_{eq}} f_f \tag{8}$$

where  $n_f$  is the number of FRP layers; and  $t_f$  is the nominal thickness of one FRP layer. In Eq. (8),  $D_{eq}$  defines the diameter of the equivalent circular cross-section for columns of square cross section with *b* edge and *r* corner radius, which can be calculated as recommended by Shayanfar *et al.* [17]:

$$D_{eq} = \frac{1 - 0.215 R_b^2}{1 - 0.215 R_b} b \tag{a9}$$

214 where

$$R_b = 2r/b \tag{b9}$$

is the corner radius ratio. Note that by using  $D_{eq}$  in the determination of FRP confinement 215 pressure, FRP volumetric ratio in the equivalent circular cross-section would be identical to 216 that of original square cross-section column. In Eq. (8),  $K_e$  is the confinement efficiency factor. 217 Shayanfar et al. [17] modified the original concept of 'confinement efficiency factor' by 218 considering the impact of concrete expansion gradient in the establishment of confinement 219 pressure, besides the well-known phenomenon of arching action. By using this concept, the 220 actual confinement pressure acting non-homogenously on the concrete is converted to an 221 equivalent confinement pressure with uniform distribution along transverse and longitudinal 222 223 directions of the column. This factor includes two components, which can be determined as suggested by Shayanfar et al. [17]: 224

$$K_e = K_H K_V \tag{10}$$

where  $K_{H}$  is the horizontal component, reflecting the influence of horizontal arching action on the distribution of confinement pressure within the cross-section of a non-circular columns (for circular columns,  $K_{H} = 1$ ), determined as:

$$K_H = R_b \ge 0.07 \tag{11}$$

In Eq. (10),  $K_v$  is the vertical component reflecting the influence of the gradient of concrete 228 lateral expansion along the column height, depending on the level of confinement stiffness (the 229 ratio of confinement pressure to concrete lateral strain). It was demonstrated by Shayanfar et 230 al. [16] that above a certain level of confinement stiffness, the confinement imposed to the 231 concrete is strong enough to strictly control the evolution of concrete expansion leading to an 232 almost null gradient along the vertical direction ( $K_v = 1$ ). However, for the cases with an 233 insufficient confinement stiffness, due to the lack of strong restriction in the curtailment of 234 concrete expansibility, the concrete column is expected to experience a highly non-235 homogenous distribution of concrete expansion and, consequently, the confinement pressure 236 in the axial loading direction is non-uniform. Shayanfar et al. [17] suggested a design-based 237 formulation to calculate  $K_V$  as follows: 238

$$K_{V} = \frac{1}{3} + \frac{2}{3}k_{\varepsilon}$$
(12)

239 in which

$$k_{\varepsilon} = 0.08 + 0.92 \left[ 2 \frac{I_f}{I_f^*} - \left( \frac{I_f}{I_f^*} \right)^2 \right] \le 1 \qquad \text{for } I_f \le I_f^*$$
(13a)

$$k_{\varepsilon} = 1$$
 for  $I_f > I_f^*$  (13b)

$$I_f^* = 0.06 + 0.0005 f_{c0} \tag{14}$$

$$I_{f} = 2K_{H} \frac{n_{f}t_{f}E_{f}\varepsilon_{c0}}{D_{eq}f_{c0}} \simeq K_{H} \frac{n_{f}t_{f}E_{f}}{550D_{eq}f_{c0}^{0.75}}$$
(15)

where  $k_{\varepsilon}$  represents the ratio of minimum and maximum concrete lateral expansion along the column height.  $I_f$  represents the confinement stiffness index regardless the influence of the gradient of concrete expansion along the column height. Finally,  $I_f^*$  is the confinement stiffness index above which  $K_V = 1$ , representing the homogenous concrete expansion along the column due to strong restrictions imposed to the concrete.

In this paper, for further simplification of the relative complexity of Eqs. (12-15) in the calculation of  $K_v$ , a simplified equation was developed based on a preliminary sensitivity analysis on the influencing factors in Eq. (12) as:

$$K_{V} = 2.2 \left( I_{f} \right)^{0.3} \le 1 \tag{16}$$

Accordingly, by using the design-based Eqs. (11, 15 and 16), the two components involved in  $K_e$  (Eq. (10)) can be calculated.

#### 250 **3-2-** Confinement pressure developed for elevated condition

Based on the model developed for ambient conditions in the previous section, the confinement pressure  $(f_{l,f}^T)$  imposed by the FRP confining stress  $(f_f)$  to HC column can be expressed as:

$$f_{l,f}^{T} = 2K_{e}^{T} \frac{n_{f}t_{f}}{D_{eq}} f_{f}^{T}$$
(17)

253 in which

$$K_e^T = K_H K_V^T \tag{18}$$

where  $K_H$  can be determined by Eq. (11). Through the substitution of confinement stiffness index of FRP confined HC columns  $(I_f^T)$  with that of FRP confined AC ones  $(I_f)$  in Eq. (16),  $K_V^T$  can be expressed as:

$$K_V^T = 2.2 \left( I_f^T \right)^{0.3} = 2.2 \beta_{0T}^{-0.45} \left( I_f \right)^{0.3} \le 1$$
<sup>(19)</sup>

in which based on Eq. (15),

$$I_{f}^{T} = K_{H} \frac{n_{f} t_{f} E_{f}}{550 D_{eq} \left(f_{c0}^{T}\right)^{0.75}} = \beta_{0T}^{-0.75} I_{f}$$
(20)

where  $\beta_{0T}$  is the axial strength ratio calculated by Eq. (2), which is equal to 1 for concrete at ambient condition; Considering that  $f_f^T$  can be calculated as  $E_f \varepsilon_h^T = E_f \varepsilon_l^T$  (where  $\varepsilon_h^T$  and  $\varepsilon_l^T$ are the generated circumferential (hoop) and radial strains, respectively, and  $E_f$  is the FRP modulus elasticity), Eq. (17) is rearranged as:

$$f_{l,f}^{T} = 2K_{e}^{T} \frac{n_{f}t_{f}}{D_{eq}} E_{f} \varepsilon_{h}^{T}$$

$$\tag{21}$$

Based on Poisson's ratio effect ( $\varepsilon_h^T = \varepsilon_l^T = v_s^T \varepsilon_c$ , where  $v_s^T$  is the secant Poisson's ratio), Eq. (21) can be rearranged as:

$$f_{l,f}^{T} = 2K_e \frac{n_f t_f}{D_{eq}} E_f v_s^{T} \varepsilon_c$$
(22)

Accordingly, in order to calculate  $f_{l,f}^{T}$  imposed to the concrete at a certain level of  $\varepsilon_{c}$ , the corresponding  $v_{s}^{T}$  is required to be addressed, which will be presented in the following section.

266

#### 267 **3-3-Dilation mechanism at elevated conditions**

During axial compressive loading, after splitting cracks have occurred, by increasing the axial 268 269 strain, the development of concrete lateral expansion abruptly increases due to Poisson's ratio effect. Experimental studies conducted by Barros and Ferreira [5], Mirmiran and Shahawy [46], 270 Lim and Ozbakkaloglu [47] and Zeng et al. [48] evidenced that the magnitude of concrete 271 272 dilatancy is strongly dependent on confinement stiffness imposed to the concrete. For the case of AC with a high level of confinement stiffness capable of limiting the evolution of concrete 273 expansion and splitting cracks, a remarkable enhancement in terms of axial strength and 274 deformability is obtained (Barros and Ferreira [5]). However, for the case of low confinement 275 stiffness, the confinement pressure imposed to the concrete is not able to overcome the concrete 276 tendency for abrupt expansion, leading to lower confinement-induced enhancements [49]. 277

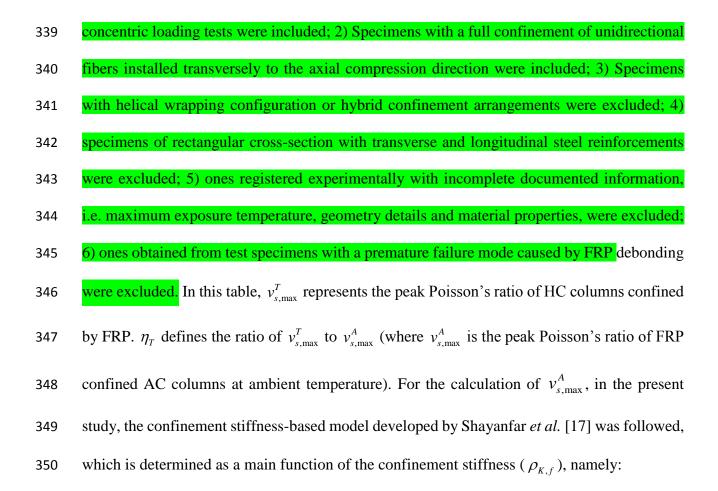
For a preliminary assessment of the dilation response of FRP confined HC columns, the 278 experimental dilation results conducted by Ouyang et al. [12] are analyzed. All tests were 279 280 conducted with specimens of diameter and height of 150 mm and 300 mm, respectively. The 281 unconfined concrete compressive strength at the ambient condition was reported 45.1 MPa. Basalt FRP (BFRP) was used with the values of thickness, modulus of elasticity and rupture 282 strain of 0.121 mm, 108.3 GPa and 2.18%, respectively. The HC columns were subjected 283 initially to various levels of maximum temperature (200 °C, 400 °C, 600 °C and 800 °C). Then, 284 they were fully confined with two and four layers of BFRP. Fig. 4 demonstrates the 285 experimental dilation responses of BFRP confined HC specimens reported by Ouyang et al. 286 [12]. Here,  $\varepsilon_v$  is the volumetric strain determined as  $\varepsilon_v = \varepsilon_c - 2\varepsilon_l = (1 - 2v_s)\varepsilon_c$  in which  $v_s$  is 287 the secant Poisson's ratio as  $v_s = \varepsilon_l / \varepsilon_c$ . Moreover, the negative and positive values of  $\varepsilon_v$ 288 represent volumetric expansion and contraction, respectively. To better demonstrate the 289 contribution of thermal-induced damage level in terms of dilation behavior, the model 290

developed by Shayanfar *et al.* [8 and 17] was followed to determine the dilation results associated with FRP confined AC specimens (*T25-L2* and *T25-L4* with red solid lines). Note that Ti-Lj refers to the concrete column heated up to the i-th maximum exposure temperature (Ti) and then, confined by j layers of BFRP.

As can be seen in Fig. 4, for all cases, regardless the level of thermal-induced damage, initial 295 296 behavior up to transition zone is virtually the same. However, beyond the transition zone, there is a noticeable difference between the transverse expansibility of HC and AC specimens. Fig. 297 298 4a reveals that at a certain axial strain ( $\varepsilon_c$ ), lateral strain ( $\varepsilon_l$ ) for the cases of T200-L2 and T400-L2 was obtained significantly higher than that of T25-L2, demonstrating the effect of 299 thermal damage on increase of  $\varepsilon_i$ . Likewise, from Fig. 4b, T200-L2 and T400-L2 have 300 experienced a large incremental volumetric expansion. However, in the T25-L2, beyond 301  $\varepsilon_c = 0.008$ , a considerable decrease in the magnitude of the increase in volumetric strain ( $\varepsilon_v$ ) 302 with respect to  $\varepsilon_c$ , followed by a reverse in volumetric evolution around  $\varepsilon_c$  =0.02, reveals the 303 capability of the confinement system imposed to AC column (T25-L2) in limiting the 304 transverse expansibility of AC columns. Likewise, as demonstrated in Fig. 4c, for T25-L2, due 305 to the adequate activated confinement imposed to AC column to overcome its tendency for 306 lateral expansibility, beyond the peak stage,  $v_s$  trend followed a decreasing branch. Even 307 308 though, heat-induced expansion for HC columns leads to an earlier activation in passive confining system of T200-L2 and T400-L2, the applied confinement was not adequate to 309 strongly constrain the concrete expansion evolution, based on its abrupt increase in  $v_s$  after 310 transition zone. On the other hand, for the cases subjected to high level of temperature (T600-311 L2 and T800-L2), as shown in Fig. 4a, at a certain level of  $\varepsilon_1$ , T600-L2 and T800-L2 312 experienced a larger axial deformation depending on thermal damage level, compared to T25-313 L2, T200-L2 and T400-L2. Likewise, Fig. 4b reveals that up to a certain level of axial strain, 314

the changes in volumetric evolution for T600-L2 and T800-L2 were almost marginal, while 315 they underwent large axial deformations. Nonetheless, above this axial strain level, as a 316 consequence of the degeneration of micro- into meso- and macro-cracks along with heat-317 induced damage in the concrete, the volumetric change evolution was suddenly reversed 318 triggering an abrupt increase in volumetric expansion. Fig. 4c also shows that for T600-L2 and 319 T800-L2, compared to the other cases, larger axial strains were obtained for a certain Poisson's 320 321 ratio. Furthermore, a closer evaluation of the data demonstrates that the maximum secant Poisson's ratio decreases significantly with increasing thermal damage, which can be attributed 322 323 to the substantial contribution of the heat-induced damage level in the establishment of dilation behavior of HC. Accordingly, by applying a certain level of axial loading, the heat-induced 324 damage leads to an additional axial strain in HC columns, and alters their transverse 325 326 expansibility, dependent strongly on thermal damage level. The comparison of dilation responses shown in Fig. 4a and Fig. 4d confirms a significant reduction in terms of lateral strain 327 by increasing FRP thickness (confinement stiffness), predominantly beyond the transition 328 zone. Fig. 4e reveals that an increase in confinement stiffness leads to shorter volumetric 329 expansion due to the stronger restrictions imposed to the concrete expansibility. The relations 330 of  $v_s$  and  $\varepsilon_c$  shown in Fig. 4f also confirms this behavior, where the specimens with more FRP 331 thickness experienced a lower value of  $v_s$  than those with less thickness (Fig. 4c). 332

In this study, it is aimed to extend the dilation model of Shayanfar *et al.* [8,17] originally suggested for FRP confined AC specimens to the case of FRP confined HC column through formulating the relation between  $v_s^T$  and  $\varepsilon_c$  at different levels of heat-induced damage  $(T_m)$ based on regression analysis. For this purpose, a dataset of the dilation responses obtained from existing experimental data was collected as presented by Table 7. It should be noted that the following criteria were adopted to include/exclude experimental data: 1) ones obtained from



$$v_{s,\max}^{A} = \frac{0.25}{\left(1 + L_{d0}/D_{eq}\right)\sqrt{\rho_{K,f}}}$$
(23)

### in which (by considering Eqs. (10), (15) and (16))

$$\rho_{K,f} = K_V I_f = K_e \frac{n_f t_f E_f}{550 D_{eq} f_{c0}^{0.75}}$$
(24)

$$0.57 \le \frac{L_{d0}}{\sqrt{A_g}\psi_f} = 1.71 - 3.53 \times 10^{-5} A_g \le 1.36$$
<sup>(25)</sup>

$$\psi_f = \frac{6.3}{\sqrt{f_{c0}}} \le 1$$
(26)

where  $L_{d0}$  is the compression damage zone length of unconfined concrete columns which was determined as recommended by Lertsrisakulrat *et al.* [50];  $A_g$  is the total area of the column's cross section.

For the determination of  $v_{s,\max}^T$ , it can be considered as a function of  $v_{s,\max}^A$  by

$$v_{s,\max}^{T} = \frac{v_{s,\max}^{T}}{v_{s,\max}^{A}} v_{s,\max}^{A} = \eta_{T} v_{s,\max}^{A}$$
(27)

Therefore, by calculating  $v_{s,\max}^{A}$  using Eq. (23) for the specimens assembled in the database, their corresponding values of  $\eta_{T}$  can be obtained as  $\eta_{T}^{Exp} = v_{s,\max}^{T} / v_{s,\max}^{A}$  (Table 7). Fig. 5a shows the variation of  $\eta_{T}^{Exp}$  with respect to  $T_{m}$ . As can be seen, by increasing  $T_{m}$  in the interval 25–400 °C,  $\eta_{T}^{Exp}$  significantly increases up to the peak, while for  $T_{m} > 400$  °C, a noticeable reduction of  $\eta_{T}^{Exp}$  with the increase of  $T_{m}$  is observed. Based on the best-fit relation obtained from regression analysis performed on 78 experimental data, the following equation was derived for determining  $\eta_{T}$  from  $T_{m}$  and  $R_{b}$  (Fig. 5a):

$$\eta_T = \frac{33.2 \left(\frac{T_m}{1000}\right)^3 - 51 \left(\frac{T_m}{1000}\right)^2 + 21.2 \left(\frac{T_m}{1000}\right) - 0.49}{1.65 - 0.65 R_b} \ge 1 \qquad \text{for } T_m \le 100 \text{ °C}$$
(28a)

$$\eta_T = \frac{33.2 \left(\frac{T_m}{1000}\right)^3 - 51 \left(\frac{T_m}{1000}\right)^2 + 21.2 \left(\frac{T_m}{1000}\right) - 0.49}{1.65 - 0.65R_b} \le 2 \qquad \text{for } 100 \text{ }^\circ\text{C} < T_m \le 800 \text{ }^\circ\text{C}$$
(28b)

where the developed expression is valid for  $T_m \le 800$  °C based on the interval of the submitted maximum exposure temperatures ( $T_m = [25 \text{ °C}, 800 \text{ °C}]$ ) in the database used for the regression analysis. Therefore, by addressing  $v_{s,\text{max}}^A$  and  $\eta_T$  in Eq. (27) through Eqs. (23, 28), the peak Poisson's ratio of FRP confined HC columns  $(v_{s,max}^T)$  can be calculated. Fig. 5b evaluates the performance of Eq. (27). Based on the obtained assessment indicators, the established expression revealed a good predictive performance.

For the determination of Poisson's ratio of HC columns confined by FRP ( $v_s^T$ ) during axial loading,  $v_s^T$  is considered as a function of  $v_{s,\text{max}}^T$ , resulting in

$$v_s^T = \frac{v_s^T}{v_{s,\max}^T} v_{s,\max}^T = \eta_\varepsilon v_{s,\max}^T$$
(29)

where  $\eta_{\varepsilon}$  represents the ratio of  $v_s^T$  and  $v_{s,\max}^T$  at a given axial strain ( $\varepsilon_c$ ). Introducing Eq. (27) into Eq. (29),  $v_s^T$  is suggested by

$$v_s^T = \eta_\varepsilon \eta_T v_{s,\max}^A \tag{30}$$

To calculate  $v_s^T$  by Eq. (30),  $\eta_{\varepsilon}$  needs to be addressed as an input parameter. For the determination of  $\eta_{\varepsilon}$  at a given level of  $\varepsilon_c$  for FRP confined AC columns (at ambient condition), Shayanfar *et al.* [8] proposed a simple but reliable multilinear model as shown in Fig. 6a. in this figure,  $c_0 c_1, c_2, c_3, c_4$  and  $c_5$  are the calibration factors reflecting the influence of confinement stiffness on  $\eta_{\varepsilon}$  versus  $\varepsilon_c$  relation;  $\varepsilon_{c,m}$  represents the axial strain corresponding to  $v_{s,max}^A$ ;  $v_{s,0}$  is the initial Poisson's coefficient of unconfined AC columns, which was determined by (Candappa *et al.* [51]):

$$v_{s,0} = 8 \times 10^{-6} f_{c0}^{2} + 2 \times 10^{-4} f_{c0} + 0.138$$
(31)

As can be seen in Fig. 6a, the pre- and post-peak phases are dependent of  $\rho_{K,f}$ . The pre-peak relation demonstrates that concrete initially behaves similar to unconfined AC column with initial Poisson's coefficient as  $v_{s,0}$ . Afterward ( $\varepsilon_c > \varepsilon_{c0}$ ),  $\eta_{\varepsilon}$  increases up to the peak stage (  $\eta_{\varepsilon} = 1$ ) at  $\varepsilon_{c,m}$ . The post-peak relation shows that  $\eta_{\varepsilon}$  decreases with the increase of  $\varepsilon_c$ , whose reduction magnitude is dependent on  $\rho_{K,f}$ . In the present study, the relation developed by Shayanfar *et al.* [8] was extended for the case of FRP confined HC columns. For this purpose, as presented in Fig. 6b, a new relation of  $\eta_{\varepsilon}$  versus  $\varepsilon_c$  was developed where the influence of thermal damage was reflected by the parameter  $\beta_{\varepsilon}$ .

$$\beta_{\varepsilon} = \beta_{\rho} \left( \varepsilon_{c0}^{T} - \varepsilon_{c0} \right) \tag{32}$$

388 in which

$$0.4 \le \beta_o = 11 \rho_{K,f}^{0.75} \le 1.4 \tag{33}$$

Accordingly, by calculating  $\beta_{\varepsilon}$  through Eq. (32),  $\eta_{\varepsilon}$  at a given  $\varepsilon_{c}$  can be obtained from the data presented in Fig 6b. Then, the corresponding  $v_{s}^{T}$  can be calculated by Eq. (30). To evaluate the reliability of the proposed relation, the results obtained from the experiments conducted by Ouyang *et al.* [12] and those determined by Eq. (30) are compared Fig. 7. As can be seen, the model has a good agreement with the experimental counterparts.

- To obtain  $\varepsilon_l^T$  versus  $\varepsilon_c$  response of FFCC-H/FFSC-H based on the developed dilation model, the calculation procedure is summarized as:
- **1.** Determine  $K_e$  using Eqs. (10), (11) and (16)
- 397 **2.** Determine  $\rho_{K,f}$  using Eq. (24)
- 398 **3.** Determine  $v_{s,\max}^A$  using Eqs. (23)
- 399 **4.** Determine  $\eta_T$  using Eq. (28)

- 400 5. Assume a value for axial strain ( $\varepsilon_c$ )
- 401 **6.** Determine  $\beta_{\varepsilon}$  using Eqs. (32), (5) to (7)
- 402 7. Determine  $\eta_{\varepsilon}$  using the developed multilinear model in Fig. 6b
- 403 **8.** Determine  $v_s^T$  using Eq. (29)
- 404 **9.** Determine  $\varepsilon_l^T$  as  $\varepsilon_l^T = v_s^T \varepsilon_c$
- 405 **10.** Continue the steps 5 to 9 up to the aim maximum value of  $\varepsilon_c$ , resulting a  $\varepsilon_l^T$  versus  $\varepsilon_c$ 406 relation.

For the assessment of the model capability in the prediction of dilation response, Fig. 8 compares  $\varepsilon_l^T$  versus  $\varepsilon_c$  relations extracted from the experimental tests conducted by Ouyang *et al.* [12] and those simulated by the proposed model. As shown, the experimental results were simulated suitably by the model confirming its reliable predictive performance.

#### 411 4- Axial Compressive Stress-strain Relation

Fig. 9 demonstrates the remarkable influence of the exposure temperature on the axial response 412 of HC columns fully confined by FRP, tested by Bisby et al. [4] and Ouyang et al. [12]. As can 413 be seen in Fig. 9a for the case of the results reported by Bisby et al. [4], compared to T25-L1 414 (control experimental specimen), even though T300-L1 experienced a slight heat-induced 415 reduction in terms of initial axial stiffness, it showed higher axial strength and deformability. 416 For T500-L1, heat- induced damage did not lead to a significant difference in the axial stress 417 versus axial strain relationship. However, for the case of severely heat-damaged specimens 418 (T686-L1), there is a noticeable reduction in its axial stiffness, compared to T25-L1. Moreover, 419 the axial stress versus axial strain relationship of T686-L1 was almost linear, compared to 420 almost bi-linear curves of specimens with the exposure temperatures lower than or equal to 500 421 °C. From the secant axial stiffness versus axial strain curves in Fig. 9b, T25-L1, T300-L1 and 422

423 T500-L1 presented a reduction of the axial stiffness during the axial compressive loading. However, in T686-L1, after an initial relatively small reduction of the stiffness, it was preserved 424 almost constant during the loading process, a consequence of the confinement effect provided 425 426 by the FRP. The assessment of the exposure temperature effects on the test specimens conducted by Ouyang et al. [12] revealed that the axial strength and stiffness of specimens 427 subjected up to 400 °C were higher than of T25-L2. It can be attributed to earlier activation of 428 confining system in the cases of HC than AC due to the increase of concrete expansibility 429 430 caused by the heat-induced damage. However, by increasing the temperature above that limit of 400 °C, thermal-induced damage increases significantly the axial deformation of the 431 concrete specimen, converting a bi-linear stress-strain response into a linear one (Fig. 9c), and 432 consequently an almost constant axial stiffness during axial loading process (Fig. 9d). 433 Accordingly, the experimental results presented in Fig. 9 evidence the imperious impact of 434 exposure maximum temperatures on the axial stress-strain response of FRP confined HC 435 columns. 436

In order to calculate the axial stress versus axial strain relationship ( $f_c^A$  vs  $\varepsilon_c$  curve) of FRP 437 passively confined AC columns (passively-confined-concrete), Active Confinement Approach 438 (i.e. [14-17, 52-54] can be followed. In this approach, the axial response of concrete with 439 440 passive confinement is derived based on that of actively-confined-concrete subjected to a constant confinement pressure during the entire axial loading history. Accordingly,  $f_c^A$ 441 corresponding to  $\varepsilon_c$  at a certain level of FRP confinement pressure  $(f_{l,f}^{A})$  can be calculated 442 by adopting an axial stress-strain base relation model ( $f_c^A = g_1(f_{cc}^A, \varepsilon_c)$ ) coupled with an axial 443 strength model, also known as failure surface function,  $(f_{cc}^{A} = g_2(f_{l,f}^{A}))$  developed for 444 actively-confined-concrete. Here,  $f_{cc}^{A}$  is the peak axial strength of axial stress-strain base 445

relation model (defined from function  $g_1$ ). However, since actively-confined-concrete case is 446 under a constant  $f_{l,f}^{A}$  during the entire axial loading history, contrary to passively-confined-447 concrete, the studies [15-17] evidenced that the original Active Confinement Approach 448 overestimates the FRP-induced enhancement of passively-confined-concrete, which is 449 generally recognized as Confinement Path Effect. To consider this effect, by adopting functions 450  $g_1$  and  $g_2$  from those exclusively developed for actively-confined-concrete, Lim and 451 Ozbakkaloglu [15] recommended a reduction factor in the confinement-induced enhancements 452 obtained for actively-confined-concrete, by decreasing the level of the confinement pressure 453  $f_{l,f}^{A}$  in the function  $g_2$ . Shayanfar *et al.* [16 and 17] proposed a new axial strength framework 454 model (function  $g_2$ ) exclusively suggested for passively-confined-concrete to predict 455 enhancements offered by a passive confining system. 456

In the present paper, for the calculation of  $f_c^A$  and  $\varepsilon_c$  relation of FRP confined AC columns taking into account *confinement path effect*, the model developed by Shayanfar *et al.* [17] presenting a unified character for both full and partial confinement configurations and both circular and square cross-sections, is followed. In this model, the axial stress-strain base framework ( $f_c^A$  versus  $\varepsilon_c$  relation using function  $g_l$ ) is given by:

$$f_{c}^{A} = f_{cc}^{A} \frac{\left(\varepsilon_{c}/\varepsilon_{cc}^{A}\right)n_{A}}{n_{A} - 1 + \left(\varepsilon_{c}/\varepsilon_{cc}^{A}\right)^{n_{A}}}$$
(34)

462 in which

$$\frac{f_{cc}^{A}}{f_{c0}} = 1 + \frac{R_{l}}{R_{2}} \left(\frac{f_{l,f}^{A}}{f_{c0}}\right)^{R_{2}}$$
(35)

$$\frac{\varepsilon_{cc}}{\varepsilon_{c0}}^{A} = 1 + 5 \left( \frac{f_{cc}}{f_{c0}}^{A} - 1 \right)$$
(36)

$$n_{A} = \frac{E_{c}}{E_{c} - \frac{f_{cc}}{\varepsilon_{cc}}^{A}} \approx \frac{1}{1 - 2.1 \times 10^{-4} \psi_{A}} \ge 1.1$$
(37)

$$\Psi_A = \frac{f_{cc}^{\ A}}{\varepsilon_{cc}^{\ A} \sqrt{f_{c0}}}$$
(38)

where  $f_{cc}^{A}$  and  $\varepsilon_{cc}^{A}$  are the peak axial strength and its corresponding axial strain, calibrated based on experimental AC specimens with passively confining system;  $R_1$  and  $R_2$  are the calibration factors in the determination of  $f_{cc}^{A}$ ;  $n_A$  is the concrete brittleness at the ambient condition depending on  $\psi_A$ , as recommended by Carreira and Chu [55]. Accordingly, at a certain level of  $\varepsilon_c$ ,  $f_{cc}^{A}$  can be determined as a function of  $f_{l,f}^{A}$  based on Eq. (35), and  $\varepsilon_{cc}^{A}$ can be, subsequently, calculated by Eq. (36), as input parameters for the determination of  $f_{c}^{A}$ by Eq. (34).

In this study, the model developed by Shayanfar *et al.* [17] was extended to be applicable for the establishment of axial response of the concrete being subjected to a certain exposure temperature. Accordingly, by substituting the mechanical characteristics of HC column with those of AC column, at a certain level of  $\varepsilon_c$  leading to FRP confinement pressure  $(f_{l,f}^T)$ , axial stress-strain base relation model  $(f_c^T$  versus  $\varepsilon_c$  curve using function  $g_l$ ) can be expressed as:

$$f_c^T = f_{cc}^T \frac{\left(\varepsilon_c / \varepsilon_{cc}^T\right) n_T}{n_T - 1 + \left(\varepsilon_c / \varepsilon_{cc}^T\right)^{n_T}}$$
(39)

475 in which

$$n_T = \frac{1}{1 - 2.1 \times 10^{-4} \psi_T} \ge 1.1 \qquad \text{for } T_m \le 400 \text{ °C}$$
(40a)

$$n_T = 2 - \frac{1 - 4.2 \times 10^{-4} \psi_T}{1 - 2.1 \times 10^{-4} \psi_T} \left( 2 - \frac{T_m}{400} \right) \ge 1.1 \qquad \text{for } 400 \ ^\circ\text{C} \le T_m \le 800 \ ^\circ\text{C}$$
(40b)

$$\Psi_T = \frac{f_{cc}^T}{\varepsilon_{cc}^T \sqrt{f_{c0}^T}} \tag{41}$$

where  $f_{cc}^{T}$  and  $\varepsilon_{cc}^{T}$  are the peak axial strength and its corresponding axial strain at a certain 476 level of  $\varepsilon_c$  as input parameters for the axial stress-strain base relation model.  $n_T$  is the concrete 477 brittleness that considers the influence of the maximum exposure temperature on  $f_{cc}^{T}$ ,  $\varepsilon_{cc}^{T}$  and 478  $f_{c0}^{T}$  through the parameter  $\psi_{T}$ . Note that the axial stiffness of FRP confined HC columns with 479 severe thermal-induced damages ( $T_m \simeq 600-800$  °C) seems to be almost constant with a linear 480 axial behavior during axial loading as demonstrated in Fig. 9. Accordingly, in the present study, 481  $n_T$  corresponding to  $T_m = 800$  °C was assumed equal to a constant value of  $n_T = 2$  during the 482 entire loading history, adjusted based on the best-fit relation of the proposed model with the 483 484 experimental axial stress-strain responses reported by Bisby et al. [4], Lenwari et al. [10], Ouyang et al. [12] and Song et al. [13]. Consequently, in Eq. (40b) (400 °C  $\leq T_m \leq 800$  °C), 485  $n_T$  was considered on the interval of the  $n_T$  obtained from Eq. (40a) for  $T_m = 400$  °C and 486  $n_T = 2$  corresponding to  $T_m = 800$  °C, with a linear relationship with  $T_m$ . 487

For the establishment of  $\varepsilon_{cc}^{T}$  at high temperatures, the preliminary comparative assessment of the proposed model with  $\varepsilon_{cc}^{T}$  obtained based on Eq. (36) demonstrated a very significant underestimation in its model predictive performance, particularly for the cases with severe thermal-induced damages. On the other hand, based on experimental studies it was evidenced that the axial behavior of FRP confined HC columns tends to be similar to actively-confined493 concrete due to more expansive behavior of HC than AC (Fig. 4). Therefore, the  $\varepsilon_{cc}^{T}$  of HC 494 columns with high exposure temperature is calculated according to the approach proposed by 495 Lim and Ozbakkaloglu [41], exclusively developed for the case of actively-confined-concrete:

$$\varepsilon_{cc}^{T} = \varepsilon_{c0}^{T} \left[ 1 + 5 \left( \frac{f_{l,f}^{T}}{f_{c0}^{T}} - 1 \right) \right] \qquad \text{for } T_{m} \ge 100 \text{ }^{\circ}\text{C}$$

$$(42a)$$

$$\varepsilon_{cc}^{T} = \varepsilon_{c0}^{T} + 0.045 \left(\frac{f_{l,f}^{T}}{f_{c0}^{T}}\right)^{1.15} + \lambda_{\varepsilon} \qquad \text{for 100 } ^{\circ}\text{C} \le T_{m} \le 200 \ ^{\circ}\text{C} \qquad (42b)$$

$$\varepsilon_{cc}^{T} = \varepsilon_{c0}^{T} + 0.045 \left(\frac{f_{l,f}^{T}}{f_{c0}^{T}}\right)^{1.15} \qquad \text{for } T_{m} \ge 200 \text{ }^{\circ}\text{C}$$

$$(42c)$$

496 in which

$$\lambda_{\varepsilon} = \left[ 0.045 \left( \frac{f_{l,f}^{T}}{f_{c0}^{T}} \right)^{1.15} - 5\varepsilon_{c0T} \left( \frac{f_{l,f}^{T}}{f_{c0}^{T}} - 1 \right) \right] \left( \frac{T_{m}}{100} - 2 \right)$$
(43)

In this study, a new axial strength model was developed, applicable to FRP confined HC
columns, having a unified character with Eq. (35) when the concrete is under ambient
conditions:

$$\frac{f_{cc}^{T}}{f_{c0}^{T}} = 1 + \frac{R_{1}}{R_{2}} \left( \frac{m}{m} \frac{f_{l,f}^{T}}{f_{c0}^{T}} \right)^{R_{2}} + \frac{R_{3}}{R_{4}} \left( \frac{f_{l,f}^{T}}{f_{c0}^{T}} \right)^{R_{4}}$$
(44)

where  $R_1$ ,  $R_2$ ,  $R_3$  and  $R_4$  are the calibration factors in the determination of  $f_{cc}^T$  obtained from the regression analyses on FRP passively confined HC columns;  $\overline{m}$  is the calibration factor reflecting the influence of more expansive behavior of the concrete with a certain level of thermal damage, which activates earlier the confining system compared to the AC column at ambient temperature (based on the comparative assessment on the dilation behavior of FFCC- 505 H/FFSC-H presented in Fig. 4). In Eq. (44), the second term  $\left(\frac{R_1}{R_2}\left(\frac{m}{m}\frac{f_{l,f}^T}{f_{c0}^T}\right)^{R_2}\right)$  represents the

improvements obtained from the confinement of an AC column with axial strength equal to  $f_{c0}^{T}$ , considering the effect of earlier activation (through  $\overline{m}$ ) compared to AC; The third term (

508  $\frac{R_3}{R_4} \left( \frac{f_{l,f}^T}{f_{c0}^T} \right)^{R_4}$  ) in Eq. (44) considers the increase of confinement-induced improvements due to 509 thermal-induced damage. Based on experimental axial stress versus axial strain relations, 510 Shayanfar *et al.* [17] proposed new expressions to determine the calibration factors of  $R_1$  and 511  $R_2$ , which was rearranged by substituting  $f_{c0}$  by  $f_{c0}^T$ :

$$R_{1} = \frac{23.9}{\beta_{0T}^{0.5} \lambda_{fc} \lambda_{Rb}} \rho_{K,f}^{0.67} \le 4.25$$
(45)

$$R_2 = \frac{1.85}{\beta_{0T}^{0.2}} \rho_{K,f}^{0.26} \ge 0.3 \tag{46}$$

512 in which

$$\lambda_{fc} = 0.75 + 0.008\beta_{0T}f_{c0} \tag{47}$$

$$\lambda_{Rb} = 1.5 \left( 1 - 1.1 R_b \right) \ge 1 \tag{48}$$

where  $\lambda_{fc}$  and  $\lambda_{Rb}$  reflect the impact of concrete axial strength and the dimension of corner radius in the calibration of  $R_1$ , respectively. In order to determine the calibration factors of  $R_3$ and  $R_4$  representing the effect of thermal-induced damage in terms of confinement-induced enhancements, the experimental axial stress-strain responses reported by Bisby *et al.* [4], Lenwari *et al.* [10], Ouyang *et al.* [12] and Song *et al.* [13] were used for statistical modeling. 518 Through regression analyses on the assembled data, the calibration factors  $R_3$  and  $R_4$  are 519 determined from:

$$R_3 = \frac{\lambda_T}{\lambda_{rb}\lambda_K} \ge 0 \tag{49}$$

$$R_4 = 0.92 \left(\frac{f_{l,f}^T}{f_{c0}^T}\right)^{0.1}$$
(50)

520 in which

$$\lambda_T = 3.55 \left(\frac{T_m}{1000}\right) - 1.55 \ge 0 \tag{51}$$

$$\lambda_{K} = 1.15 - 0.022 K_{H} \frac{n_{f} t_{f} E_{f}}{D_{eq} f_{c0}}$$
(52)

$$\lambda_{cb} = 1.22R_b^{0.25} \ge 0.85 \tag{53}$$

where  $\lambda_T$ ,  $\lambda_K$  and  $\lambda_{rb}$  reflect the impact of maximum exposure temperature ( $T_m$ ), confinement stiffness and the dimension of corner radius in the calibration of  $R_3$ , respectively. As shown in Fig. 10a, the developed model parameter ( $\lambda_T$ ) provides a sufficient agreement with the experimental counterparts, which was determined based on the best-fit relation of the proposed model with the experimental axial stress-strain responses.

526 Due to the fact that pre-existing micro-cracks in thermally damaged concrete tend to activate 527 passively confining system at the initial stage of axial compressive loading, the calibration 528 factor of  $\overline{m}$  was considered in the establishment of Eq. (44), having been obtained from 529 regression analysis to enhance the confinement effectiveness, resulting:

$$\overline{m} = 1 + m_0 \exp\left(-11.2 \frac{f_{l,f}^T}{f_{c0}^T}\right)$$
(54)

$$m_0 = \frac{m_T}{m_\rho m_r} \tag{55}$$

$$0 \le m_T = 0.025 (T_m - 100) \le 2.5$$
 for  $T_m \le 400$  °C (56a)

$$m_T = 2.5 - 0.01 (T_m - 400) \ge 0.3$$
 for  $T_m \ge 400$  °C (56b)

$$m_r = 0.3 + 0.7R_b \tag{57}$$

$$m_{\rho} = 0.2\beta_{0T}^{0.3}\rho_{K,f}^{-0.4} \tag{58}$$

where  $m_T$ ,  $m_r$  and  $m_\rho$  are the calibration factors determined based on the regression analysis reflecting the effect of maximum exposure temperature  $(T_m)$ , corner radius ratio  $(R_b)$  and confinement stiffness  $(\rho_{K,f})$ . As shown in Fig. 10b, the developed model parameter  $(m_T)$  has a good agreement with the experimental counterparts, which extracted based on Eqs. (51 and  $-E_{TT}$ 

535 52) 
$$(m_T^{Exp} = m_\rho m_r \frac{m^{Exp} - 1}{\exp(-11.2f_{l,f}^T / f_{c0}^T)}$$
 where  $\overline{m}^{Exp}$  was determined using back analysis from

the best fit of the experimental results of the axial stress-strain curve of test specimens withthose obtained from the developed model).

#### 538 **5- Calculation Process**

539 In the following, the calculation methodology of the proposed model, which can be 540 implemented into a spreadsheet, for determining the axial response of FRP confined concrete 541 submitted to a certain level of thermal damage is presented. The calculation procedure is as:

- **1.** Determine the mechanical characteristics of unconfined heat-damaged concrete:
- Peak axial strength  $(f_{c0}^T)$  by Eq. (1)
- Axial strain corresponding to  $f_{c0}^T$  ( $\mathcal{E}_{c0}^T$ ) by Eq. (6)

545 **2.** Assume a value for  $\varepsilon_c$  on the interval  $(0, \varepsilon_{cu}]$  where  $\varepsilon_{cu}$  is the ultimate axial strain when 546 FRP rupture occurs.

- 547 **3.** Determine the dilation response corresponding to  $\varepsilon_c$
- 548 Secant Poisson's ratio  $(v_s^T)$  by Eq. (29) and the data presented in Fig. 6
- 549 Confinement pressure  $(f_{l,f}^T)$  by Eq. (22)
- 550 **4.** Determine the axial response corresponding to  $\mathcal{E}_c$
- Calibration factors  $R_1$ ,  $R_2$ ,  $R_3$  and  $R_4$ , by Eqs. (45), (46), (49), and (50)
- 552  $\overline{m}$  factor from Eq. (54)
- 553 Peak axial strength  $(f_{cc}^T)$  by Eq. (44)
- 554 Axial strain  $(\varepsilon_{cc}^{T})$  corresponding to  $f_{cc}^{T}$  by Eq. (42)
- 555 Axial stress  $(f_c^T)$  by Eq. (39)

556 **5.** Continue the aforementioned incremental procedure up to  $\varepsilon_{cu}$ ,  $f_c^T$  versus  $\varepsilon_c$  relation can 557 be calculated.

558

Since the focus of the current study was given on the simulation of global axial stress-strain curves, the experimental values of ultimate axial strain ( $\varepsilon_{cu}$ ) was used to terminate the computation process.

562 It is noteworthy that the reliability of regression analyses performed for developing predictive

563 equations (as key components of the proposed model) is limited to the range of input/output

- variables supported in the used database. Accordingly, the predictive performance of these
- sequations can be improved through recalibrating the model components based on new datasets
- 566 consisting of the relevant variables with a broader range. Furthermore, the experimental data

567	used for calibrating the failure surface function and the coupled dilation model was obtained
568	from tests on relatively small FRP confined prototypes of square/circular concrete specimens
569	where thermal distribution inside the concrete can be reasonably considered uniform.
570	Therefore, for real cases with a larger dimension and non-uniform thermal distribution whose
571	relative variables might not be in the aforementioned interval, the key components of the
572	proposed model might need to be recalibrated, which will be the focus of a future study.
573	Considering the relatively simple methodology of the proposed analytical-based model, it can
574	be extended potentially to FRP confined heat-damaged RC columns of rectangular cross-
575	section, through addressing properly the influences of dual FRP-steel confinement, sectional
576	aspect ratio (the ratio of longer and shorter cross-section dimensions) and their interactions
577	with exposure temperature in terms of axial and dilation behavior.

#### 578 **6- Verification**

This section assesses the predictive performance of the developed analysis-oriented model for the prediction of axial response of concrete specimens submitted to a certain maximum exposure temperature, and after the specimens have attained the environmental temperature, subsequently, confined with FRP confining system. For this purpose, the axial stress-strain curve obtained from the proposed model is compared to that obtained from the experimental studies conducted by Bisby *et al.* [4], Lenwari *et al.* [10], Ouyang *et al.* [12] and Song *et al.* [13].

Bisby *et al.* [4] performed an experimental study to investigate the axial stress-strain response
of FRP fully confined circular HC columns. The diameter and height of the test specimens

588 were 100 mm and 200 mm, respectively. The axial compressive strength of AC column at the room temperature was 28 MPa. The values of nominal thickness, modulus of elasticity and 589 rupture strain of CFRP jackets were reported as 0.12 mm, 241.1 GPa and 1.7%, respectively. 590 591 All the specimens submitted to a certain level of maximum exposure temperature were confined by one CFRP layer. Complete details regarding the test specimens can be found from 592 Bisby et al. [4]. Fig. 11 presents the comparison of the results obtained from the analytical 593 594 model with those measured experimentally. As can be seen, the model has a good predictive performance in the estimation of axial responses of the test specimens submitted to 300 °C, 595 500 °C and 700 °C, even though there is a slight overestimation in terms of maximum axial 596 strength for T500-L1. 597

Lenwari et al. [10] experimentally determined the axial stress-strain response of FRP fully 598 confined circular HC columns. The diameter and height of the test specimens were 150 mm 599 600 and 300 mm, respectively. The axial compressive strength of AC column at the room temperature was 40.5 MPa. The values of nominal thickness, modulus of elasticity and rupture 601 strain of CFRP jackets were reported as 0.131 mm, 234.1 GPa and 1.8%, respectively. All the 602 603 specimens submitted to a certain level of maximum exposure temperature were confined by 604 one CFRP layer. Complete details regarding the test specimens can be found from Lenwari et al. [10]. Fig. 12 demonstrates the comparison of the results obtained from the analytical model 605 with those measured experimentally. As can be seen, the model was able to predict the 606 607 experimental counterparts with a good agreement, even though there is a slight overestimation in terms of maximum axial strength for T300-L1 and T500-L1. 608

For further investigation of the capability of the developed confinement model, the axial stressstrain curves obtained from experimental studies conducted by Ouyang *et al.* [12] and Song *et al.* [13], where the test specimens were submitted to a high level of thermal-induced damage (

612  $T_m \ge 600$  °C), are compared with those analytically obtained from the model, as shown in Figs. 613 13 and 14. As can be observed, the model could accurately predict the full range of the 614 experimentally measured axial responses, except for a slight underestimation for the cases of 615 T600-L3 and T600-L3 tested by Song *et al.* [13] (Figs. 14e and f).

Due to the unified character of the proposed analysis-oriented model at ambient and elevated 616 temperature conditions, Fig. 15 compares the axial stress- strain relations of FFSC-A reported 617 from the experimental study conducted by Wang and Wu [6] with those analytically obtained 618 from the model to assess its capability for the cases at ambient condition. All specimens had a 619 section dimension of 150 mm and a height of 300 mm, with a sectional corner radius ratio ( $R_{\rm h}$ 620 621 ) varying from 0 (r = 0) to 1 (r = 75 mm) representing a square cross section with sharp edges and circular cross-section, respectively. Two series of FFSC-A specimens with concrete 622 strengths of  $f_{c0} \simeq 30$  MPa and  $f_{c0} \simeq 50$  MPa were tested. The CFRP thickness, tensile elastic 623 624 modulus and rupture strain were 0.165 mm, 219 GPa, and 1.99%, obtained from flat coupon tensile tests. The complete details of the experimental program can be found in Wang and Wu 625 [6]. As can be seen in Fig. 15, in general, there are a good agreement between the experimental 626 axial stress-strain relationships with those obtained from the proposed model, confirming the 627 successful simulation of the corner radius ratio  $(R_{h})$  influence on confinement-induced 628 629 enhancements of FFSC-A at ambient conditions.

# 630 7- Summary and Conclusion

This paper has addressed the development of a new analysis-oriented model to predict the axial and dilation behavior of FRP confined HC circular/square concrete columns. Through regression analyses performed on a large database of unconfined heat-damaged concrete experimentally tested specimens, new expressions were developed to determine its mechanical

635	characteristics in terms of axial compressive strength and its corresponding axial strain. A new
636	model was developed to determine dilation response of FRP confined HC columns by
637	formulating the effect of thermal damage level on Poisson's coefficient versus axial strain
638	relationship. Subsequently, a new axial stress-strain model, coupled with the developed dilation
639	model, was proposed to calculate the axial behavior of FRP confined HC columns with the
640	different levels of maximum exposure temperature. Comparisons with axial and dilation results
641	reported by available experiment studies in the literature verified that the developed analysis-
642	oriented model is able to predict the experimental counterparts with good accuracy, and has a
643	relatively simple format for design purposes by using a data sheet.
644	
645	
646	
647	
648	
649	
650	
651	

# 652 Data Availability Statement

653	All data and models related to the present study could be available from the corresponding
654	author upon rational request.
655	
656	
657	
658	
659	Acknowledgments
660	This study is a part of the project "StreColesf_Innovative technique using effectively composite
661	materials for the strengthening of rectangular cross-section reinforced concrete columns
662	exposed to seismic loadings and fire", with the reference POCI-01-0145-FEDER-029485. The
663	firs author also acknowledges the support provided by FCT PhD individual fellowship 2019
664	with the reference of "SFRH/BD/148002/2019".
665	
666	
667	
668	
669	
670	
671	
672	
673	
674	

## 675 **References**

- Kodur, V. (2014). Properties of concrete at elevated temperatures. International Scholarly
   Research Notices.
- Bamonte, P., & Lo Monte, F. (2015). Reinforced concrete columns exposed to standard fire:
   Comparison among different constitutive models for concrete at high temperature. Fire safety
   journal, 71, 310-323.
- 681
  3. Demir, U., Green, M. F., & Ilki, A. (2020). Postfire seismic performance of reinforced precast concrete columns. PCI Journal, 65(6).
- 683 4. Bisby, L. A., Chen, J. F., Li, S. Q., Stratford, T. J., Cueva, N., & Crossling, K. (2011).
  684 Strengthening fire-damaged concrete by confinement with fibre-reinforced polymer wraps.
  685 Engineering Structures, 33(12), 3381-3391.
- 5. Barros JA, Ferreira DR. Assessing the efficiency of CFRP discrete confinement systems for concrete cylinders. J Compos Constr 2008;12(2):134-148.
- 688 6. Wang LM, Wu YF. Effect of corner radius on the performance of CFRP-confined square
  689 concrete columns: test. Eng Struct 2008;30:493–505.
- For a strengthening technique for increasing
  Janwaen, W., Barros, J. A., & Costa, I. G. (2019). A new strengthening technique for increasing
  the load carrying capacity of rectangular reinforced concrete columns subjected to axial
  compressive loading. Composites Part B: Engineering, 158, 67-81.
- 8. Shayanfar J, Rezazadeh M, Barros JA (2020a). Analytical model to predict dilation behavior
  of FRP confined circular concrete columns subjected to axial compressive loading. J Compos
  Constr 2020;24(6):04020071.
- 696 9. Shan B, Gui FC, Monti G, Xiao Y (2019). Effectiveness of CFRP confinement and compressive
  697 strength of square concrete columns. J Compos Constr 2019 23(6):04019043
- Lenwari, A., Rungamornrat, J., & Woonprasert, S. (2016). Axial compression behavior of firedamaged concrete cylinders confined with CFRP sheets. Journal of Composites for
  Construction, 20(5), 04016027.
- 11. Luo, X., Sun, W., & Chan, S. Y. N. (2000). Effect of heating and cooling regimes on residual
  strength and microstructure of normal strength and high-performance concrete. Cement and
  Concrete Research, 30(3), 379-383.
- 704 12. Ouyang, L. J., Chai, M. X., Song, J., Hu, L. L., & Gao, W. Y. (2021). Repair of thermally
  705 damaged concrete cylinders with basalt fiber-reinforced polymer jackets. Journal of Building
  706 Engineering, 44, 102673.
- 13. Song, J., Gao, W. Y., Ouyang, L. J., Zeng, J. J., Yang, J., & Liu, W. D. (2021). Compressive
  behavior of heat-damaged square concrete prisms confined with basalt fiber-reinforced polymer
  jackets. Engineering Structures, 242, 112504.
- Teng J, Huang YL, Lam L, Ye LP. Theoretical model for fiber-reinforced polymer-confined
   concrete. J Compos Constr 2007;11(2):201-210.

- 15. Lim JC, Ozbakkaloglu T (2014a). Unified stress-strain model for FRP and actively confined
   normal strength and high-strength concrete. J Compos Constr 2014;19(4):04014072.
- Shayanfar, J., Barros, J. A., & Rezazadeh, M. (2021a). Generalized Analysis-oriented model of
   FRP confined concrete circular columns. Composite Structures, 270, 114026.
- 716 17. Shayanfar, J., Barros, J. A., & Rezazadeh, M. (2022). Unified model for fully and partially FRP
  717 confined circular and square concrete columns subjected to axial compression. Engineering
  718 Structures, 251, 113355.
- 18. Kodur, V. K. R., & Sultan, M. A. (2003). Effect of temperature on thermal properties of high strength concrete. Journal of materials in civil engineering, 15(2), 101-107.
- 19. Hertz, K. D. (2005). Concrete strength for fire safety design. Magazine of concrete research,
  57(8), 445-453.
- 20. Raut, N. K., & Kodur, V. K. R. (2011). Response of high-strength concrete columns under design fire exposure. Journal of Structural Engineering, 137(1), 69-79.
- Aslani, F., & Bastami, M. (2011). Constitutive relationships for normal-and high-strength
   concrete at elevated temperatures. ACI Materials Journal, 108(4), 355.
- 727 22. Chang, Y.F., Chen, Y.H., Sheu, M.S., and Yao, G.C. (2006). "Residual stress-strain
  728 relationship for concrete after exposure to high temperatures." Cement and Concrete Research,
  729 36, 1999–2005.
- Al-Salloum, Y. A., Elsanadedy, H. M., & Abadel, A. A. (2011). Behavior of FRP-confined
  concrete after high temperature exposure. Construction and Building Materials, 25(2), 838-850.
- 732 24. Sharma, U., Zaidi, K., & Bhandari, N. (2012). Residual compressive stress-strain relationship
   733 for concrete subjected to elevated temperatures. Journal of Structural Fire Engineering.
- 734 25. Geng, J., Sun, Q., Zhang, W., & Lü, C. (2016). Effect of high temperature on mechanical and
  735 acoustic emission properties of calcareous-aggregate concrete. Applied Thermal Engineering,
  736 106, 1200-1208.
- 737 26. Xiao, J., Li, Z., Xie, Q., & Shen, L. (2016). Effect of strain rate on compressive behaviour of
  738 high-strength concrete after exposure to elevated temperatures. Fire Safety Journal, 83, 25-37.
- 739 27. Xiang, S., Zeng, L., Zhang, J., Chen, J., Liu, Y., Cheng, G., & Mo, J. (2019). A DIC-based
  740 study on compressive responses of concrete after exposure to elevated temperatures. Materials,
  741 12(13), 2044.
- 28. Li, L. Y., & Purkiss, J. (2005). Stress-strain constitutive equations of concrete material at
  elevated temperatures. Fire Safety Journal, 40(7), 669-686.
- 744 29. Han, L. H., & Huo, J. S. (2003). Concrete-filled hollow structural steel columns after exposure
  745 to ISO-834 fire standard. Journal of Structural Engineering, 129(1), 68-78.
- 746 30. Eurocode 2: Design of Concrete Structures ENV EC2. 1992.
- 747 31. Lie, T. T., & Lin, T. D. (1985). Fire performance of reinforced concrete columns. In: ASTM
  748 STP 882. Fire Safety: Science and Engineering. p. 176–205.

749 32. Lie, T. T., Rowe, T. J., & Lin, T. D. (1986). Residual strength of fire-exposed reinforced concrete columns. Detroit: American Concrete Institute; Special Publication, 92, 153-174. 750 33. Dahl, K. K. B. (1992). "Uniaxial stress-strain curves for normal and highstrength concrete." 751 ABK Rep. No. R282, Dept. of Structural Engineering, Technical Univ. of Denmark, Kongens 752 Lyngby, Denmark. Eurocode 2: Design of Concrete Structures ENV EC2. 1992. 753 754 34. Jansen, D. C., & Shah, S. P. (1997). Effect of length on compressive strain softening of concrete. Journal of engineering mechanics, 123(1), 25-35. 755 35. Watanabe, K., Niwa, J., Yokota, H., and Iwanami, M. (2004). "Experimental study on stress-756 757 strain curve of concrete considering localized failure in compression." J. Adv. Concr. Technol., 2(3), 395–407. 758 759 36. Wei, Y., & Wu, Y. F. (2016). Experimental study of concrete columns with localized failure. 760 Journal of Composites for Construction, 20(5), 04016032. 761 37. Wu YF, Wei Y (2016). Stress-Strain Modeling of Concrete Columns with Localized Failure: 762 An Analytical Study. J Compos Constr 2016;20(3):04015071. 763 38. Yang, K. H., Lee, Y., & Mun, J. H. (2019). A Stress-Strain Model for Unconfined Concrete in Compression considering the Size Effect. Advances in Materials Science and Engineering, 764 765 2019. 39. Popovics S. A numerical approach to the complete stress-strain curve of concrete. Cement and 766 concrete research 1973;3(5):583-599. 767 40. Karthik MM, Mander JB. Stress-block parameters for unconfined and confined concrete based 768 on a unified stress-strain model. J Struct Eng 2010;137(2):270-273. 769 770 41. Lim JC, Ozbakkaloglu T (2014b). Stress-strain model for normal-and light-weight concretes under uniaxial and triaxial compression. Constr Build Mater 2014;71:492-509. 771 42. Terro, M. J., 1998, "Numerical Modeling of the Behavior of Concrete Structures in Fire," ACI 772 773 Structural Journal, V. 95, No. 2, Mar.-Apr., pp. 183-193. 43. Khennane A, Baker G. Uniaxial model for concrete under variable temperature and stress. J 774 775 Eng Mech-ASCE 1993;119(8):1507-25. 776 44. Bazant P, Chern JC. Stress-induced thermal and shrinkage strains in concrete. J Eng Mech-ASCE 1987;113(10):1493-511. 777 45. Lie TT. Structural fire protection. New York: American Society of Civil Engineers; 1992. 778 779 46. Mirmiran A, Shahawy M. Dilation characteristics of confined concrete. Mechanics of 780 Cohesive- frictional Materials: Mech Cohesive-Frict Mater 1997;2(3):237-249. 47. Lim JC, Ozbakkaloglu T (2014c). Hoop strains in FRP-confined concrete columns: 781 782 experimental observations. Mater Struct 2014;48(9):2839-2854. 783 48. Zeng, J.-J., Guo, Y.-C., Gao, W.-Y., Li, J.-Z., and Xie, J.-H. (2017). "Behavior of partially and fully FRP confined circularized square columns under axial compression." Construction and 784 785 Building Materials, 152, 319-332.

- 49. Shayanfar J, Rezazadeh M, Barros JA, Ramezansefat H (2020b). A new dilation model for FRP fully/partially confined concrete column under axial loading. The 3RD RILEM Spring Convention 2020 Ambitioning a Sustainable Future for Built Environment: Comprehensive Strategies for Unprecedented Challenges, Guimarães Portugal 2020.
- 50. Lertsrisakulrat, T., Watanabe, K., Matsuo, M., and Niwa, J. (2001). "Experimental study on parameters in localization of concrete subjected to compression." J. Mater. Concr. Struct.
  Pavement, 669(50), 309–321.
- 51. Candappa DC, Sanjayan JG, Setunge S. Complete triaxial stress-strain curves of high-strength concrete. Journal of Materials in Civil Engineering 2001;13(3):209-215.
- 52. Shayanfar, J., Rezazadeh, M., & Barros, J. A. (2021b). Theoretical Prediction of Axial
  Response of FRP Fully/partially Confined Circular Concrete Under Axial Loading. In
  International Conference on Fibre-Reinforced Polymer (FRP) Composites in Civil Engineering
  (pp. 1439-1449). Springer, Cham.
- 53. Lin, G., & Teng, J. G. (2020). Advanced stress-strain model for FRP-confined concrete in
  square columns. Composites Part B: Engineering, 197, 108149.
- 54. Yang, J., Wang, J., & Wang, Z. (2020). Axial compressive behavior of partially CFRP confined
  seawater sea-sand concrete in circular columns–Part II: A new analysis-oriented
  model. *Composite Structures*, 246, 112368.
- Solution Solution